



Process Development for High V_{oc} CdTe Solar Cells

C.S. Ferekides and D.L. Morel
University of South Florida
Tampa, Florida

NREL is a national laboratory of the U.S. Department of Energy, Office of Energy Efficiency & Renewable Energy, operated by the Alliance for Sustainable Energy, LLC.

Subcontract Report
NREL/SR-5200-51605
May 2011

Contract No. DE-AC36-08GO28308

Process Development for High V_{oc} CdTe Solar Cells

C.S. Ferekides and D.L. Morel
University of South Florida
Tampa, Florida

NREL Technical Monitor: Harin S. Ullal
Prepared under Subcontract No. XXL-5-44205-10

NREL is a national laboratory of the U.S. Department of Energy, Office of Energy Efficiency & Renewable Energy, operated by the Alliance for Sustainable Energy, LLC.

**This publication was reproduced from the best available copy
submitted by the subcontractor and received no editorial review at NREL.**

NOTICE

This report was prepared as an account of work sponsored by an agency of the United States government. Neither the United States government nor any agency thereof, nor any of their employees, makes any warranty, express or implied, or assumes any legal liability or responsibility for the accuracy, completeness, or usefulness of any information, apparatus, product, or process disclosed, or represents that its use would not infringe privately owned rights. Reference herein to any specific commercial product, process, or service by trade name, trademark, manufacturer, or otherwise does not necessarily constitute or imply its endorsement, recommendation, or favoring by the United States government or any agency thereof. The views and opinions of authors expressed herein do not necessarily state or reflect those of the United States government or any agency thereof.

Available electronically at <http://www.osti.gov/bridge>

Available for a processing fee to U.S. Department of Energy
and its contractors, in paper, from:

U.S. Department of Energy
Office of Scientific and Technical Information
P.O. Box 62
Oak Ridge, TN 37831-0062
phone: 865.576.8401
fax: 865.576.5728
email: <mailto:reports@adonis.osti.gov>

Available for sale to the public, in paper, from:

U.S. Department of Commerce
National Technical Information Service
5285 Port Royal Road
Springfield, VA 22161
phone: 800.553.6847
fax: 703.605.6900
email: orders@ntis.fedworld.gov
online ordering: <http://www.ntis.gov/help/ordermethods.aspx>

Cover Photos: (left to right) PIX 16416, PIX 17423, PIX 16560, PIX 17613, PIX 17436, PIX 17721



Printed on paper containing at least 50% wastepaper, including 10% post consumer waste.

Table of Contents

| | |
|---|-----------|
| List of Figures | iv |
| List of Tables | vi |
| 1 Introduction | 1 |
| 2 Open-Circuit Voltage (V_{oc}) | 2 |
| 3 Summary of Fabrication Procedures – Experimental Methods | 3 |
| 4 Front and Back Contact Materials | 5 |
| 4.1 Titanium Oxide (TiO_2) | 5 |
| 4.1.1 Solar Cells with Titanium Oxide Buffer | 9 |
| 4.1.2 Solar Cells with Alloyed Titanium Oxide Buffers | 11 |
| 4.2 Titanium Selenide ($TiSe_2$)..... | 12 |
| 4.2.1 Selenization of Ti Films | 12 |
| 4.3 Interfacial Dipole Layers | 13 |
| 4.3.1 Energy Band Diagram | 13 |
| 4.3.2 Interfacial Compounds & Their Application on CdTe Cells | 14 |
| 5 The Effect of CdTe Impurities on Solar Cell Performance | 19 |
| 5.1 Phosphorous (P) Incorporation in the CdTe Source Material | 19 |
| 5.2 The Effect of CSS(CdTe) Ambient | 20 |
| 5.3 Antimony (Sb) as a Potential Dopant for CdTe | 22 |
| 5.3.1 The Need for the $CdCl_2$ Heat Treatment (HT) | 23 |
| 5.3.2 The Effect of Excess “Surface-Sb” | 24 |
| 5.3.3 The Effect of the Sb-diffusion Process Parameters | 25 |
| 6 Indium (In) Doped CdS | 28 |
| 6.1 CBD-CdS Control Samples | 28 |
| 6.2 In Doping of CSS-CdS | 30 |
| 7 Measuring Collection in CdTe Cells | 31 |
| 7.1 The Effect of Collection on Solar Cell Performance | 32 |
| Appendix – Polymers Used as IFLs in CdTe Cells | 35 |
| References | 36 |

List of Figures

| | |
|--|----|
| Figure 1. SEM Images of TiO ₂ films deposited under different conditions: (a-top) reactive sputtering at room temperature; (b-middle) sputtering from TiO ₂ at 300°C; (c-bottom) reactive sputtering in O ₂ /N ₂ . NOTE: the left image magnification varies for the three films; the right image magnification is the same (see scale at the bottom of each image). Credit: University of South Florida. | 6 |
| Figure 2. XRD spectra for TiO ₂ films prepared under different processing conditions. | 7 |
| Figure 3. Light J-V characteristics of a CdTe cell fabricated with TiO ₂ as a buffer layer | 10 |
| Figure 4. Monochromatic light J-V characteristics for a CdTe cell fabricated with a TiO ₂ buffer | 10 |
| Figure 5. V _{OC} of CdTe cells with Ti-Sn-O buffers. | 11 |
| Figure 6. Light J-V for CdTe cells fabricated with TiO ₂ buffers; (V _{OC} 's of 880, 900 and 950 mV; the 900 and 950 mV cells were fabricated with "alloyed" TiO ₂) | 12 |
| Figure 7. XRD spectrum of a selenized Ti film, showing the presence of the TiSe ₂ phase | 13 |
| Figure 8. Energy Band diagrams for metal/dipole/semiconductor interfaces showing a case where the orientation of the dipole results in an apparent increase in the metal work function (a), and a case where the dipole orientation results in a decreases in the metal work function (b). | 14 |
| Figure 9. Increase in V _{OC} vs. the type of interfacial polymer (SAMs). | 16 |
| Figure 10. Light I-V and SR data for CdTe cells contacted using polymers (SAMs) as interfacial contact layers; Mo/SAM/CdTe/CdS. | 18 |
| Figure 11. V _{OC} and FF for CdTe cells fabricated from a CdTe:P CSS source | 20 |
| Figure 12. The effect of the CSS-CdTe deposition ambient on the V _{OC} and FF of CdTe solar cells..... | 20 |
| Figure 13. Dark J-V characteristics (left: ln(J)-V; right: J-V) for representative cells fabricated under various N ₂ /O ₂ mixtures (total pressure 10 torr) during the CSS-CdTe deposition..... | 21 |
| Figure 14. Light J-V characteristics of the CdTe cells of Fig. 11 | 21 |
| Figure 15. Sample arrangement used for the Sb diffusion experiments. Credit: University of South Florida..... | 23 |
| Figure 16. Light J-V (left) and SR data (right) for representative CdTe;Sb cells from table 9..... | 24 |

| | |
|--|----|
| Figure 17. Light (left) and dark (right) I-V for representative CdTe cells from table 10..... | 25 |
| Figure 18. Light J-V for representative cells from table 11..... | 26 |
| Figure 19. Doping profiles (from C-V measurements) for the cells shown in Fig. 18 (table 11)..... | 26 |
| Figure 20. The SR of CdTe;Sb cells fabricated with different Sb-diffusion temperatures..... | 26 |
| Figure 21. Light J-V (left) and doping profile (right) of CdTe cells fabricated with and w/o Sb-diffusion..... | 27 |
| Figure 22. Methods used to incorporate indium in CdS..... | 28 |
| Figure 23. SR data for CdTe cells fabricated with CBD-CdS:In window layers (see table 12)..... | 29 |
| Figure 24. V_{OC} and FF for cells with CSS-CdS deposited in the presence of oxygen | 31 |
| Figure 25. V_{OC} and FF for cells with CSS-CdS deposited in inert ambient | 31 |
| Figure 26. SR data for the cells of Figs 24 (left) and 25 (right) | 31 |
| Figure 27. Monochromatic light J-V data for two “typical” CdTe solar cells..... | 32 |
| Figure 28. FF as a function of wavelength of the monochromatic light (data from Fig 27)..... | 32 |
| Figure 29. Collection functions for various wavelengths; the data for 640 and 700 nm are fitted with polynomials. | 33 |
| Figure 30. Collection functions for 640 and 700 nm and their effect on the light I-V of an otherwise “ideal” solar cell..... | 34 |

List of Tables

| | |
|---|----|
| Table 1. Summary of processes and materials utilized for the fabrication of CdTe solar cells | 4 |
| Table 2. XRD data for the TiO ₂ films shown in Fig. 2; “A” and “R” in the ID column identify the Anatase and Rutile phases of TiO ₂ respectively..... | 8 |
| Table 3. The highest V _{OC} (for the identified deposition conditions) obtained for CdTe/CdS cells fabricated on TiO ₂ buffer layers | 9 |
| Table 4. XRD data for the film with XRD spectrum shown below..... | 13 |
| Table 5. Polymers in Tetrahydrofuran  as solvent..... | 14 |
| Table 6: Polymers in Ethanol as solvent..... | 15 |
| Table 7: Procedures for polymer application and cell fabrication..... | 15 |
| Table 8. Net carrier concentration and depletion width for the cells shown in Figs 13 &14 | 22 |
| Table 9. Process conditions and solar cell results for CdTe:Sb cells; the effect of the CdCl ₂ HT | 24 |
| Table 10. Process conditions and performance data for CdTe:Sb cells; the effect of HCl etch | 25 |
| Table 11. Process conditions/solar cell results for CdTe:Sb cells; the effect of annealing time | 26 |
| Table 12. CdTe Solar Cells fabricated with CBD-CdS films as-deposited and doped with Indium..... | 29 |
| Table 13. Effect of collection on the FF | 34 |

1 Introduction

This is a **cumulative and final report for Phases I, II and III** of this NREL funded project (subcontract # XXL-5-44205-10)). The main activities of the project focused on **the open-circuit voltage of the CdTe thin film solar cell**. Although, CdTe continues to be one of the leading materials for large-scale cost-effective production of photovoltaics, the efficiency of the CdTe solar cell has been stagnant for the last few years. At the manufacturing front, the CdTe technology is fast paced and moving forward with US-based First Solar Inc. leading the world in CdTe module production, and poised to become the largest PV manufacturer in the world. In order to support industrial efforts and continue the advancement of this technology it will be necessary to continue improvements in solar cell efficiency. A closer look at the present state-of-the-art performance levels puts the three solar cell efficiency parameters, short-circuit current (J_{SC}), open-circuit voltage (V_{OC}), and fill factor (FF) in the 24-26 mA/cm², 840-850 mV, and 74-76% ranges respectively. During the late 90's efforts to improve cell efficiency were primarily concerned with increasing J_{SC} , simply by utilizing thinner CdS window layers in order to enhance the blue response (<510 nm) of the CdTe cell, which lead to the development of “buffers” (or high resistivity transparent films) [1-4]. The use of transparent bi-layers (low- ρ /high- ρ), as the front contact is becoming a “standard” feature of the CdTe cell.

Quantifying the losses in the typical CdTe superstrate structure reveals that J_{SC} has approached its practical limits, much more so than V_{OC} and FF, which is the reason that recently the CdTe community has been turning its attention to V_{OC} as the focus of efforts driven by higher efficiency goals [5].

This report describes and summarizes the results from this 3-year project.

2 Open-Circuit Voltage (V_{OC})

Improving V_{OC} in the typical CdTe/CdS p-n heterojunction solar cell is not straightforward as a practical matter, due to several reasons. The greatest challenge faced by CdTe researchers is the fact that the CdTe cell components (and fabrication processes) have significant interdependencies and cannot be easily decoupled. Thus making both the fabrication and understanding of device operation for CdTe cells complex. For example, copper (Cu) was initially believed to be a key element for the formation of the back contact, until studies of impurity distribution in CdTe/CdS solar cells indicated that this element accumulates at the junction interface, where it also impacts the device performance/characteristics [6,7,8]. Work at USF that focused on incorporating Cu at the interface and not at the back contact, suggested that some Cu concentration at the junction interface (and in CdS) is required in order to achieve high performance [7,9]. Another example of the interdependence between cell components and processing is the effect of the CdCl₂ heat treatment, or “activation” process (which is a standard fabrication step). This process is known to have three major effects on the CdTe solar cell: (a) CdTe grain enhancement; (b) enhanced interdiffusion between CdTe and CdS (that leads to the formation of a mixed Cd_{1-x}S_xTe crystal at the junction interface); (c) defect passivation/lifetime improvement via the formation of Cl-related complexes in CdTe. The extent to which these changes take place depends on the fabrication history/properties of the CdTe/CdS structure. Grain enhancement is predominant in small grain (<1 μm approx.) CdTe films, with large grain films (>1 μm approx.) undergoing little or no grain growth. Interdiffusion in CdTe/CdS junctions, during the activation process, is typically less when these are deposited at high temperatures (>500°C typ.). Therefore, the process of improving the V_{OC} (and in general the performance) of CdTe cells is complicated by these interdependencies.

As already indicated above, the focus of this project is on the V_{OC} of the CdTe solar cell. Improving this parameter will require new materials, device configurations, and possibly advanced fabrication techniques. Moving V_{OC} beyond the present state-of-the-art 850 mV mark will require improvements/changes in one or more of the following: (a) recombination; it is believed that recombination is the dominant transport mechanism at the junction, and therefore reducing the recombination levels (i.e. reducing J_0) could lead to higher V_{OC} ; (b) doping levels; the magnitude of V_{OC} is related to the built-in potential of the junction, which is determined by the doping levels in the heterojunction partners. Therefore increasing the doping level (in particular in CdTe) could lead to higher V_{OC} 's; (c) back contact barrier; it has been shown via several modeling efforts that the back contact energy can also affect V_{OC} . Depending on the doping levels in CdTe, the band bending (and therefore V_{OC}) in this layer can be determined by the energy of the back contact. Therefore large work function contact materials could also lead to improved V_{OC} ; (d) front contact/buffer: empirical evidence suggests that the front contact can also have a significant influence V_{OC} , and therefore alternative front contact materials (buffers) could also play a key role in improving this device parameter.

The main objective of this project was to develop materials/processes that will lead to the advancement of the open-circuit voltage of CdTe solar cells; the main areas investigated were:

1. impurities in the CdTe absorber: the focus in this case was on controlling the net hole concentration in CdTe, the ultimate objective being to increase the doping in this layer and therefore the built-in voltage (and V_{OC});
2. high-work function back contact materials;

3. improved front contact: in this case the focus was on investigating new buffer layers, as well as studying the effect of impurities in CdS;
4. back contact development; a new approach to improve the back contact of the CdTe cell by using interfacial dipoles was explored.

3 Summary of Fabrication Procedures – Experimental Methods

The solar cell fabrication processes utilized during this project are summarized in Table 1. The close-spaced sublimation (CSS) was used for the deposition of all CdTe films. Although this process is well known for its high throughput (deposition rates over 1 $\mu\text{m}/\text{min}$ are easily achievable), it is not very suitable for dopant incorporation; for this project (as it will be discussed later) an attempt was made to incorporate the dopant in the source material. Cadmium sulfide window layers were deposited by two methods: (a) chemical bath deposition (CBD), and (b) CSS. To-date no attempt has been made to incorporate a dopant during the CBD process (this is an option being considered for future activities); Indium was used as a dopant for CSS-CdS films.

As already discussed above, Cu is an important element used for the fabrication of CdTe solar cells. For certain tasks of this project Cu was eliminated from all solar cell fabrication steps, in order to decouple the effects of the various impurities being studied.

It should also be noted that during the early stages of this project the baseline TCO material (i.e. CVD-SnO₂) was temporarily unavailable, due to the prohibitively high costs of the fluorine (F) doping source (Halocarbon 13B1 or bromotrifluoromethane CBrF₃). Instead sputtered indium-tin oxide (ITO) and SnO₂ were used as the front contact bi-layer (ITO/SnO₂). No significant effects on device performance were identified as a result of this change.

Solar cells were characterized using standard techniques for light and dark current-voltage (J-V), spectral response (SR), and capacitance-voltage (C-V) characteristics. Materials characterization including x-ray diffraction spectroscopy (XRD), energy dispersive x-ray spectroscopy (EDS), and scanning electron microscopy (SEM) were also used on an as-needed basis. Secondary Ion Mass Spectroscopy (SIMS) and Auger analysis are being carried out in collaboration with NREL.

Table 1. Summary of processes and materials utilized for the fabrication of CdTe solar cells

| | Materials | COMMENTS |
|------------------------------|-----------------------------|--|
| Substr. | 7059 Borosilicate Glass | Borosilicate glass cleaned in dilute HF solution (1:10) and rinsed with DI water |
| Transparent Contact | SnO ₂ :F | by MOCVD (Tetramethyltin, O ₂ , F-source: Halocarbon 13B1) |
| | ITO | by sputtering of In ₂ O ₃ :Sn @ T _{SUB} =300°C, or co-sputtering of In ₂ O ₃ and SnO ₂ |
| Buffer Layer (high-p) | SnO ₂ | by MOCVD (as above; undoped) |
| | SnO ₂ | by sputtering of Sn (reactive) or SnO ₂ targets |
| | TiO ₂ and Alloys | by sputtering; from TiO ₂ or Ti (reactive sputtering) |
| CdS | | by: (a) Chemical Bath Deposition (CBD) and (b) Close-spaced sublimation (CSS); (5N) |
| CdTe | CdTe (5N) | by CSS |
| CdCl₂ HT | CdCl ₂ (4N) | Direct application of CdCl ₂ onto CdTe by evaporation followed by heat treatment |
| Back Contact | Polymers | Used as interfacial layers (IFL) between CdTe and the metallic electrode |
| | Graphite | (a) doped with HgTe:Cu; (b) undoped (used as received) |
| | Mo | by RF sputtering |

4 Front and Back Contact Materials

Among the main tasks of this project is the study of new materials for both the back and front contacts of the CdTe cell. Titanium dioxide (TiO_2) – a material previously considered by the CdTe national Team – was studied and incorporated as a buffer in CdTe cells; titanium selenide (TiSe_2), a large work function material [10,11], was investigated as a back contact candidate. This section provides a description of the processing and material properties of these two materials.

4.1 Titanium Oxide (TiO_2)

Sputtering of a ceramic TiO_2 target in argon (Ar), and reactive sputtering of a metallic Ti target (in Ar/ O_2 ambient) were used for the deposition of TiO_2 films. The substrate temperature was varied from RT to 300°C. In some cases N_2 was also added to the gas mixture. The electrical resistivity for all TiO_2 films was too high to measure with conventional (4-point probe) means. The film structural properties were studied using XRD and SEM. Figure 1 shows representative SEM images for films deposited using:

- a) reactive sputtering from a Ti target (top);
- b) sputtering from a TiO_2 target (middle);
- c) sputtering in the presence of N_2 (bottom).

In all instances the grain size ranges from 100-200 nm; however, the “grains” in films (a) and (b) appear to be clusters of smaller particles, unlike film (c) where the grains appear to be better developed; also film (c) appears to be relatively more porous.

X-ray diffraction analysis of TiO_2 films revealed that reactively-sputtered as-deposited at room temperature films (similar to film (a) in Fig. 1), exhibited poor crystallinity – dark blue data in Fig. 2; the same was found to be true for films deposited at higher substrate temperatures from TiO_2 (similar to film (b) in Fig. 1) not shown in Fig. 2. The crystallinity of these films appears to improve when they are heat-treated at high temperatures (over 600°C) in air – green and purple data in Fig. 2. The remaining film in Fig. 2 (orange data) was deposited with N_2 in the sputtering ambient at a substrate temperature of 250°C. Table 2 lists the peaks identified for the various films in Fig. 2. In all cases the films appeared to contain both TiO_2 phases (i.e. anatase and rutile).

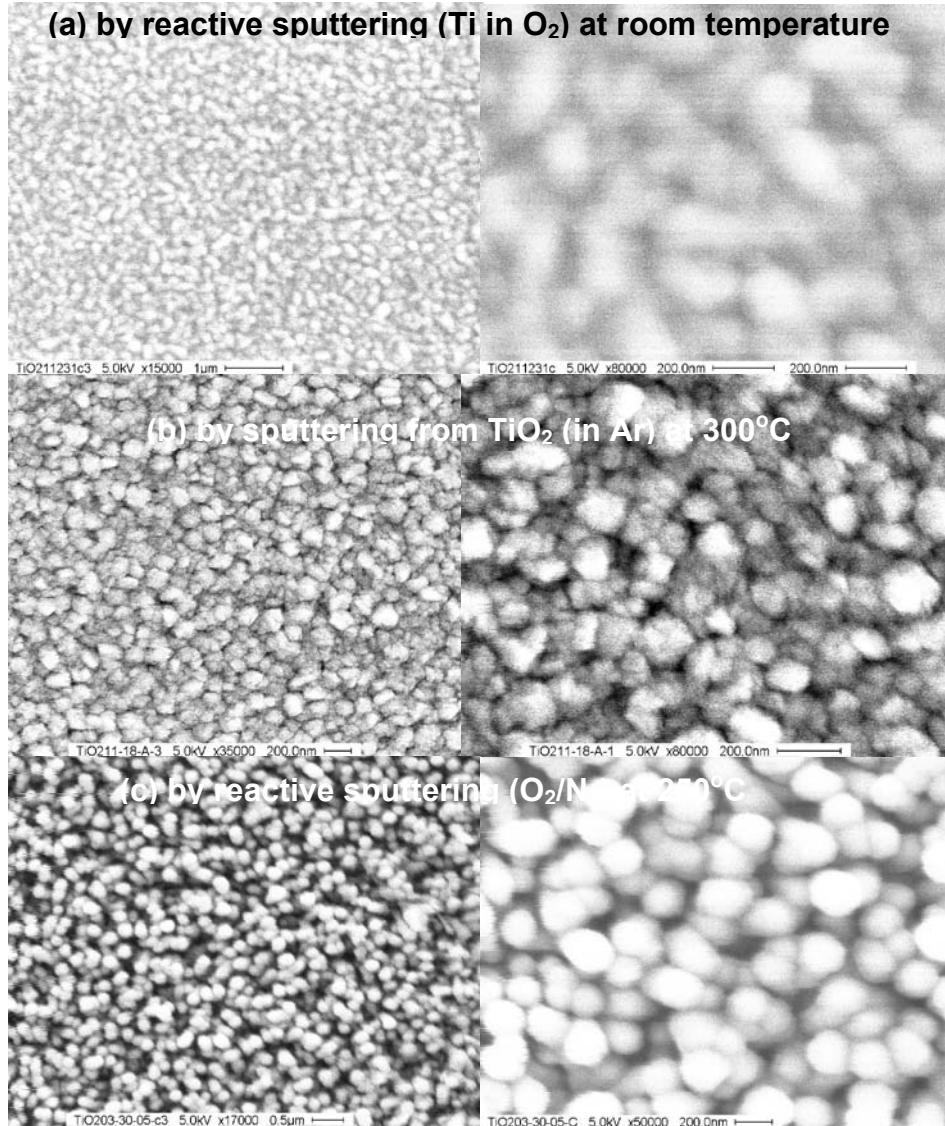


Figure 1. SEM Images of TiO₂ films deposited under different conditions:
 (a-top) reactive sputtering at room temperature; (b-middle) sputtering from TiO₂ at 300°C; (c-bottom) reactive sputtering in O₂/N₂. **NOTE:** the left image magnification varies for the three films; the right image magnification is the same (see scale at the bottom of each image).
 Credit: University of South Florida.

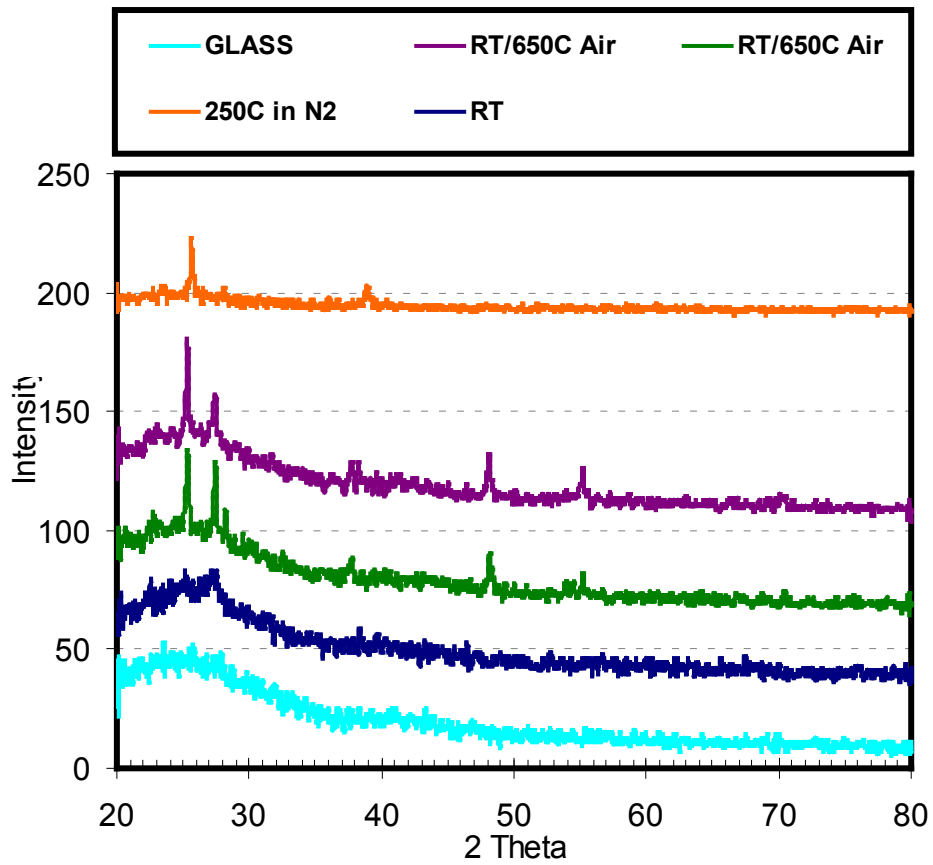


Figure 2. XRD spectra for TiO₂ films prepared under different processing conditions.

Table 2. XRD data for the TiO₂ films shown in Fig. 2; “A” and “R” in the ID column identify the Anatase and Rutile phases of TiO₂ respectively

| Sample | 2 Theta [°] | d-spacing [Å] | FWHM | Rel. Int. [%] | ID |
|--|-------------|---------------|--------|---------------|---------|
| T_{DEP}=RT | 25.329 | 3.5164 | 0.2362 | 89.65 | (101) A |
| Ann. 650°C/Air | 27.422 | 3.2526 | 0.1181 | 100 | (110) R |
| (green data) | 48.179 | 1.8888 | 0.3149 | 38.26 | (200) A |
| | 54.593 | 1.6797 | 2.304 | 6.49 | (211) A |
| T_{DEP}=RT | 25.346 | 3.5141 | 0.1574 | 100 | (101) A |
| Ann. 650°C/Air | 27.343 | 3.2617 | 0.4723 | 45.44 | (110) R |
| (purple data) | 48.105 | 1.8915 | 0.2362 | 43.45 | (200) A |
| | 55.18 | 1.6632 | 0.576 | 24.81 | (211) A |
| T_{DEP}=250°C (O₂&N₂) | 25.626 | 3.4763 | 0.1181 | 100 | (101) A |
| (orange data) | 38.908 | 2.3148 | 0.4723 | 33.66 | (200) R |

4.1.1 Solar Cells with Titanium Oxide Buffer

Titanium oxide films were incorporated in solar cell structures as buffers:

SnO₂:F/TiO₂/CdS/CdTe/Back contact.

The cell processing characteristics for the devices fabricated with TiO₂ buffers were:

- Front contact:
 - CVD - SnO₂:F
 - *TiO₂ by sputtering (process variations listed in table below)*
- CdS: by Chemical bath deposition (thickness: 90-100 nm)
- CdTe: by the close-spaced sublimation (thickness: 5-6 μm)
- CdCl₂-heat treatment @ 390°C
- Back Contact:
 - Doped graphite annealed @ 250°C[†]

Table 3 lists *the highest* V_{OC} values obtained for cells fabricated using TiO₂ as a buffer. In one of these instances where the cells were fabricated on TiO₂ sputtered in the presence of N₂ a V_{OC} of 880 mV was measured. Nevertheless, the overall cell behavior for these devices was very poor, and results are notably noisy with significant data scattering in particular of the V_{OC} .

Table 3. The highest V_{OC} (for the identified deposition conditions) obtained for CdTe/CdS cells fabricated on TiO₂ buffer layers

| TiO ₂ Deposition Conditions | | | | | V_{OC} [mV] | FF Range [%] |
|--|---------------------|---------------------|--------|-------------------|------------------|-----------------|
| Ar [mT] | N ₂ [mT] | O ₂ [mT] | T [°C] | Thickness [nm] | | |
| 4.5 | 1.5 | - | 180 | 30 | 880 | 5-25 |
| 4.5 | 1.5 | - | 180 | 10 | 840 | 8-27 |
| 4.5 | 1.5 | - | 180 | 20 | 790 | 13-22 |
| 1 | - | 4 | 250 | 30 | 780 | 10-12 |
| - | - | 5 | 250 | 30 | 820 | 7-9 |

[†] These contacts contain Cu

The light J-V characteristics of all TiO₂-based solar cells were very similar, with FF's always being less than 25%; an example is shown in Fig. 3. This J-V behavior suggests strong collection in reverse bias (J_L is in the range of 22-23 mA/cm²); however, J_L collapses near zero volts leading to the poor FF and poor overall cell performance. This is believed to be due to the high resistivity of TiO₂. If the cause for this collapse in collection is better understood it is possible that TiO₂ buffers can provide a viable option for fabricating higher V_{OC} CdTe solar cells.

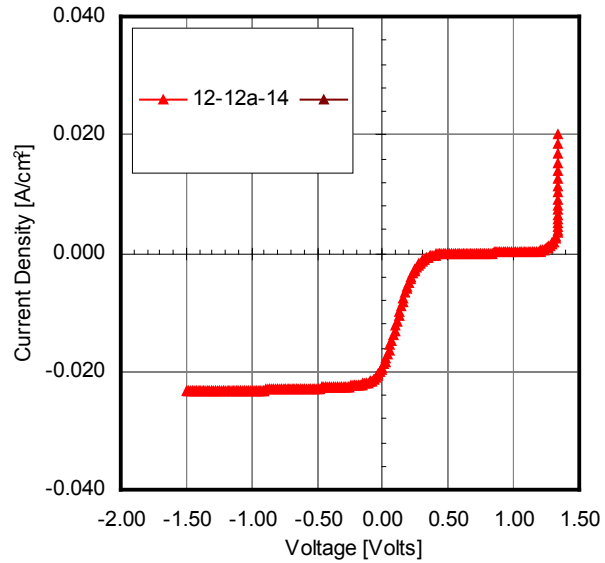


Figure 3. Light J-V characteristics of a CdTe cell fabricated with TiO₂ as a buffer layer

Carrier collection in TiO₂-based solar cells was evaluated using “monochromatic” J-V measurements, where the complete J-V characteristics of solar cells were measured using interference filters (with 20 nm bandwidth), with the intensity of the light source adjusted to correspond to AM1.5 (within the specific wavelength range)⁷. Results from this measurement, for one of the samples that exhibited V_{OC} near 900 mV, are shown in Fig. 4. Qualitatively, there appear to be no significant changes in the overall shape of the light J-V, suggesting that collection within CdTe is to first order independent of bias and wavelength.

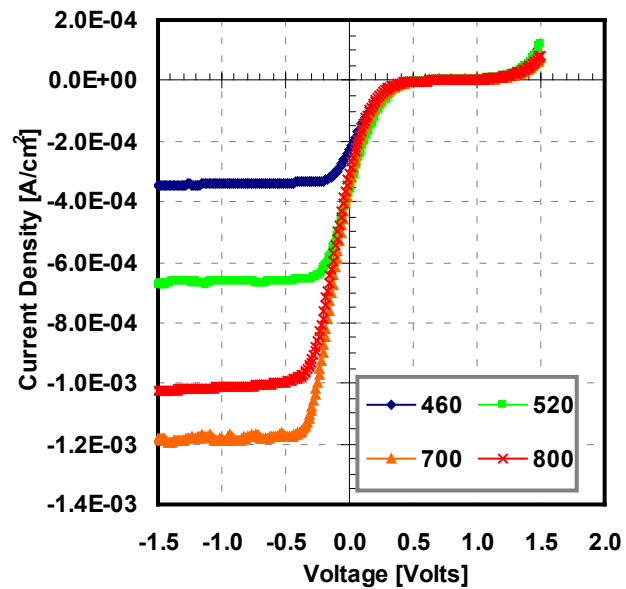


Figure 4. Monochromatic light J-V characteristics for a CdTe cell fabricated with a TiO₂ buffer

Although, based on the overall solar cell results measured to date, some general trends were observed (i.e. as a function of TiO₂ processing conditions), the spread of the results (both V_{OC} and FF) was in most cases very large and no conclusions could be drawn on how variations in the properties of the TiO₂ films influence cell performance. This behavior points to the possibility that (non-uniform) micro-diode effects play a critical role in the observed solar cell behavior. Another common behavior observed during this study is that within the same substrate (i.e. identically processed devices) increases in V_{OC} were accompanied with decreases in the FF.

⁷ A discussion on using monochromatic J-V measurements to estimate efficiency losses due to inefficient collection is included later in this report.

4.1.2 Solar Cells with Alloyed Titanium Oxide Buffers

As indicated in the previous section the high resistivity of TiO_2 is suspected to be one of the reasons for the poor J-V characteristics associated with devices with TiO_2 buffers. During the latter parts of Phase II, TiO_2 films were revisited in order to determine whether their properties (specifically resistivity) could be controlled with alloying. To this date, TiO_2 films have been alloyed with other commonly used transparent oxides (ZnO and SnO_2).

Film resistivity has not been affected by alloying (films remain too resistive to measure with a 4-point probe); nevertheless, alloying appears to have an effect on the V_{OC} of the device, with the overall J-V shape remaining unchanged (same as Fig. 3). The data shown in Fig. 5 show the V_{OC} as a function of the amount of Sn in the Ti-Sn-O alloys; the values corresponding to $\text{Sn}/(\text{Sn}+\text{Ti})$ of 20% have exhibited V_{OC} 's in the 900-950 mV range. It has been mentioned previously that there is significant scattering in the V_{OC} of cells with TiO_2 buffers; this remains the case for the results shown in Fig. 5; however, it should be noted that the data is from 3 different experiments, and in all instances the high V_{OC} substrates (i.e. samples with $\text{Sn}/(\text{Sn}+\text{Ti})=20\%$) yielded cells with V_{OC} of at least 900 mV, suggesting that the alloying effects can be reasonably reproduced. Figure 6 compares J-V characteristics from high V_{OC} cells fabricated with TiO_2 -based buffers (includes TiO_2 alloyed with SnO_2). The arrows in the figure mark the shift in the J-V curves as V_{OC} increases. As mentioned previously one of the observed trends in these devices was a decrease in the FF with increasing V_{OC} . Alloying TiO_2 with ZnO has resulted in lower V_{OC} s independent of the $\text{Zn}/(\text{Zn}+\text{Ti})$ ratio.

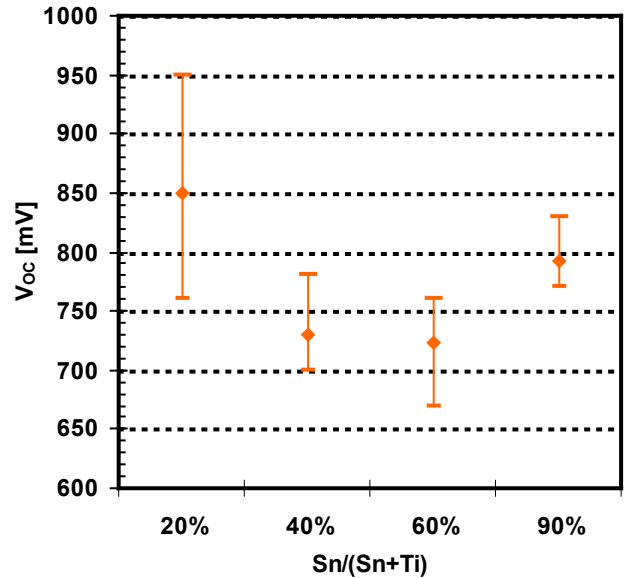


Figure 5. V_{OC} of CdTe cells with Ti-Sn-O buffers.

Although, much remains to be understood about the role of buffers, in particular TiO_2 -based films, it appears that they do “influence” the V_{OC} of CdTe cells; therefore buffers should remain as one of the viable methods to increase this solar cell parameter. The challenge still remains identifying the important buffer properties, and “tuning” them for optimum solar cell (V_{OC}) performance.

4.2 Titanium Selenide (TiSe₂)

As part of the task that addresses the characteristics of the back contact of the CdTe solar cell, this project focused on the investigation of a promising class of materials, layered compound metals, which combine high chemical inertness with high work function and metallic conductivity. These properties make these materials good candidates for the back contact electrode. Chemical inertness is desired to limit chemical reactions at the interface with CdTe, and high work function is required to enable the formation of ohmic contacts (the CdTe layers are typically p-type, i.e. a hole injecting contact is needed). Potential layered compound candidates are the selenides TiSe₂, VSe₂, NbSe₂ and TaSe₂, as well as their corresponding sulfides.

4.2.1 Selenization of Ti Films

Based on the existing deposition facilities the decision was made to investigate TiSe₂ films; early efforts focused on preparing this compound by selenizing Ti. Metallic Ti films were sputter-deposited on glass slides to a thickness of 200-400 Å, and subsequently exposed to a Se flux under high vacuum conditions; the selenization process was carried out in a CIGS chamber which contained excess Se. It was found that the formation of TiSe₂ by this method depends on the substrate temperature. For temperatures below 400°C no TiSe₂ was detected. The Ti films appeared (visual inspection) to change color at temperatures around 400°C. At selenization temperatures of 425°C the TiSe₂ phase was detected; this can be seen in Fig. 7 where the xrd spectrum of a Ti selenized film clearly shows diffraction peaks that have been found to correspond to TiSe₂. Table 4 lists the identified peaks and compares them to pdf data.

While Ti selenization resulted in TiSe₂ films it was not possible to prepare this compound on CdTe with this approach. Efforts to selenize Ti films deposited directly on CdTe have to-date failed due to the fact that the selenization conditions (elevated substrate temperature/high vacuum) cause the partial evaporation of CdTe.

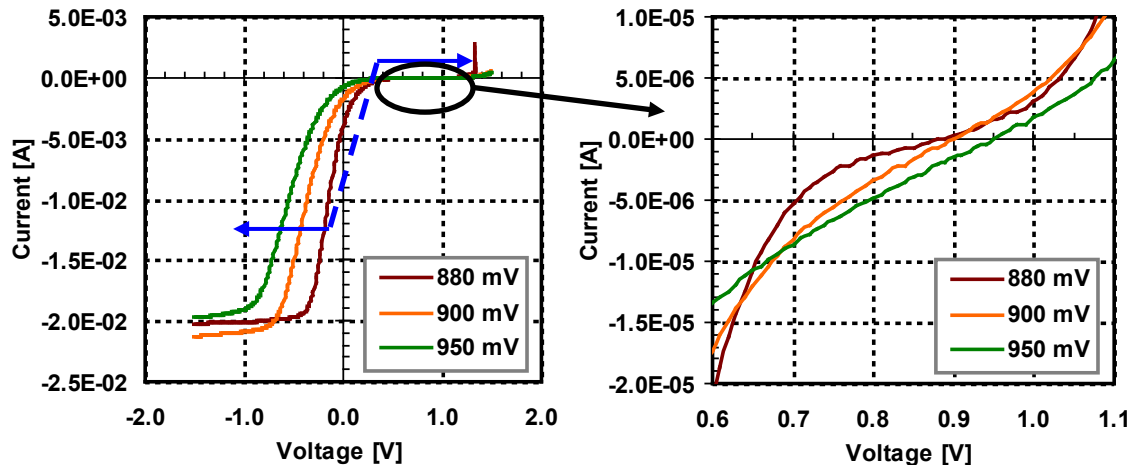


Figure 6. Light J-V for CdTe cells fabricated with TiO₂ buffers; (V_{OC}'s of 880, 900 and 950 mV; the 900 and 950 mV cells were fabricated with "alloyed" TiO₂)

4.3 Interfacial Dipole Layers

During the last phase of this project a novel method of forming back contacts to CdTe solar cells was investigated. The approach has been used in organic devices and has shown promise in modifying the work function of metals and transparent contacts. Using self-assembled monolayers (SAMs) or layers of dipole polymers, the work function of silver was modified from 3.8 to 5.5 eV using alkanethiols[16]. For this project we collaborated with Dr. Peter Zhang of the Department of Chemistry at USF; Dr. Peter Zhang is an expert in the synthesis of organic compounds, and his group synthesized all compounds used for this part of the project.

4.3.1 Energy Band Diagram

The use of an interfacial dipole can be used to improve the contact characteristics by modifying the band alignment. Figure 8 shows the two scenarios where a metal comes in contact with a p-type semiconductor via an interfacial dipole. For the case depicted on the left, the polarity of the dipole is in a direction that results in an “effective metal work function” higher than what the actual work function of the metal, and on the right the situation is reversed (i.e. the “effective work function” is lower). For CdTe solar cells the scenario depicted on the left would be beneficial since it would help improve the p-type contact by effectively increasing the metal work function.

Table 4. XRD data for the film with XRD spectrum shown below

| This work | | PDF 01-083-0980 – TiSe ₂ | | |
|-----------|------------------|--|------------------|-----------------|
| 2θ [°] | d-spacing [Å] | 2 θ [°] | d-spacing [Å] | % Difference |
| 14.646 | 6.0483 | 14.742 | 6.004 | 0.7% |
| 29.6473 | 3.0133 | 23.138 | 3.06227 | 1.6% |

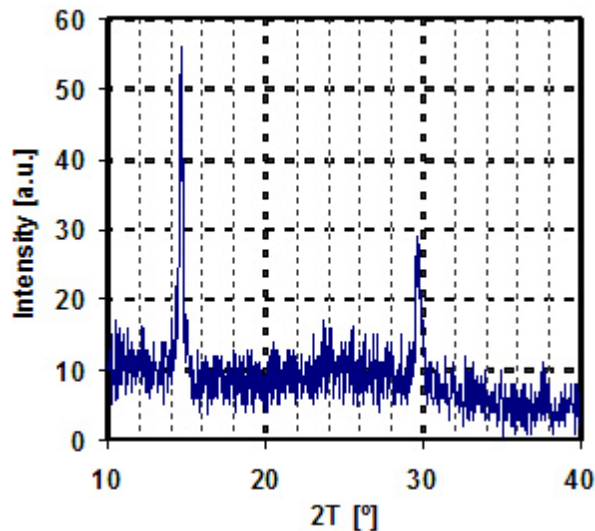


Figure 7. XRD spectrum of a selenized Ti film, showing the presence of the TiSe₂ phase

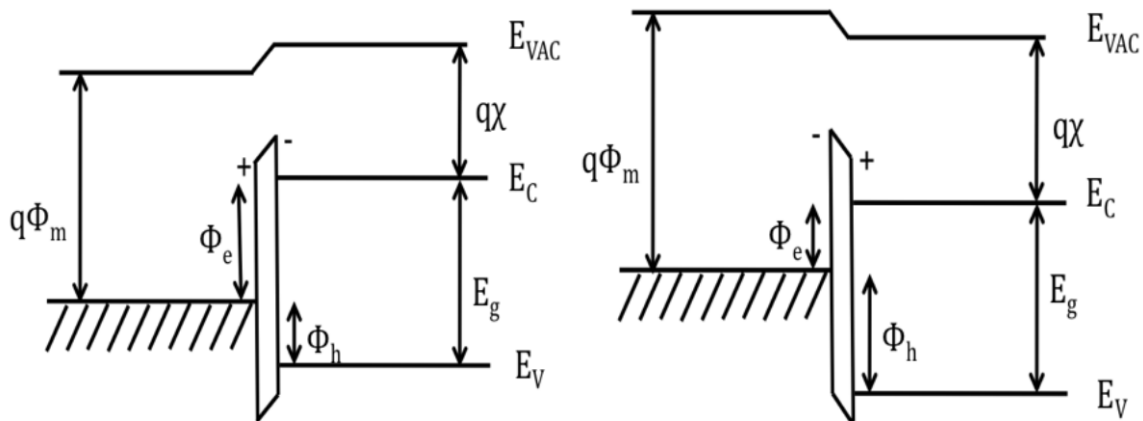


Figure 8. Energy Band diagrams for metal/dipole/semiconductor interfaces showing a case where the orientation of the dipole results in an apparent increase in the metal work function (a), and a case where the dipole orientation results in a decreases in the metal work function (b).

4.3.2 Interfacial Compounds & Their Application on CdTe Cells

Several organic compounds were synthesized and dissolved in two different solvents (tetrahydrofuran and some in ethanol). The intent was to compare compounds that would result in different polarity (i.e. would tend to favor one of the two cases considered in Fig. 8) and also have different dipole strengths. The table below shows lists the various organic compounds synthesized for this study.

Table 5. Polymers in Tetrahydrofuran  as solvent

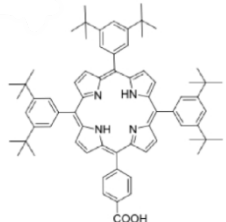
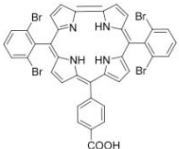
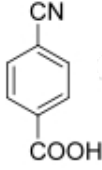
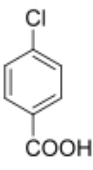
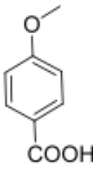
| Sample# | Polymer name | Chemical Formula | Concentration [mol/L] | Polymer Structure | Relative dipole strength |
|---------|--------------|--------------------------|-----------------------|---|--------------------------|
| 1 | IV-283-1B | $C_{69}H_{78}N_4O_2$ | 0.005 |  | Electro-negative |
| 2 | V-100-1 | $C_{38}H_{22}Br_4N_4O_2$ | 0.005 |  | Electro-negative |

Table 6: Polymers in Ethanol as solvent

| Sample# | Polymer name | Polymer chemical formula | Concentration [mol/L] | Polymer structure | Relative dipole strength |
|---------|-------------------------------------|--|-----------------------|---|--------------------------|
| 1 | IV-284-1A IV-284-1B IV-284-1C | C ₈ H ₅ NO ₂ | 200 100 50 |  | Electro-positive |
| 2 | IV-212A | C ₇ H ₅ ClO ₂ | 0.2 |  | Electro-positive |
| 3 | p-Anisic acid | C ₈ H ₈ O ₃ | 0.05 |  | Electro-negative |

The above-described compounds were spin-coated onto the surface of CdTe (which had been previously CdCl₂ treated, rinsed and etched to remove surface impurities and oxides) prior to depositing Mo by sputtering. The application process was developed in-house empirically using guidance from literature. Speed, acceleration, total time, a 2-step vs. 1-step spin coating process, and the amount of material dispensed were optimized to result in uniform coatings. A total time of 50-60 seconds and a speed of 1500 rpm, were found to be the most critical spin coating parameters to produce uniformly spread 1 drop of solution and dry the solvent. Following the application of the polymers, the samples were loaded into the vacuum chamber for the deposition of Mo; prior to the Mo-deposition the samples were heated at 100°C for 15 minutes to remove all remaining solvent. The table listed below includes key process parameters for cell fabrication and polymer application:

Table 7: Procedures for polymer application and cell fabrication

| | Cell Fabrication | Polymer Spin Coating |
|---|--|-----------------------------|
| 1 | SnO ₂ ; MOCVD bi-layer | rpm=1500 |
| 2 | CdS; CBD | Acceleration=3 [†] |
| 3 | CdTe; CSS (4-5 μm) | Time=1 min |
| 4 | CdCl ₂ HT | Solution volume=1 drop |
| 5 | Rinse and etch (in Br ₂ /methanol soln) | |

The first series of experiments were performed on samples fabricated as described in table 7 (no Cu intentionally added at any step of the cell fabrication process). Figure 9 shows the change in V_{OC} from a reference sample (i.e. no polymer used); it should be noted that all V_{OC}s for these cells were very poor (300-550 mV). The two reasons for the low V_{OC}s are believed to be the absence of Cu, and the potential presence of pinholes in the CBD CdS films; the CdS-CBD

[†] Spin coater setting (1-5)

process is being re-evaluated as it appears to be generating a large amount of powder in solution, something that was not present in the past. The result of this is thinner films and increased pinhole concentration.

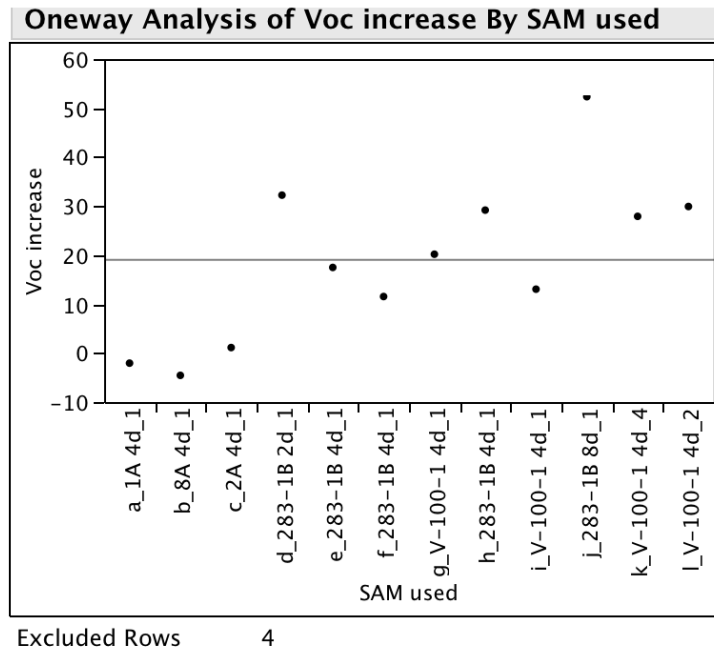


Figure 9. Increase in V_{oc} vs. the type of interfacial polymer (SAMs).

Based on the results shown in Fig. 9 some general trends have been observed; note that the second to last number in the sample IDs shown in Fig. 9 designate the number of drops dispensed (i.e. ...2d, ...4d, ...8d) during the application and is therefore expected to produce a thicker polymer film.

1. Compounds 283-1B and V-100-1 showed consistent and the largest increase in terms of V_{OC} (approx. a 52% increased for sample 283-1B 8d_1). Qualitatively, these were expected to yield higher V_{OC} s based on the potential strength and alignment of the dipole formed.
2. The use of a larger number of drops produced higher V_{OC} s. This behavior may be due to more complete coverage of the surface of CdTe with the polymer films, or an increased thickness of the polymer.
3. Increasing the amount of solution used resulted in more uniform cell-to-cell results on the same substrate; this may also suggest complete and uniform coverage as mentioned in step 2.

Light I-V and SR data for a set of samples are shown in Fig. 10 below; the V_{OC} as indicated above is much lower than the 850 mV state-of-the-art values (in the 500 mV range); a roll over in the first quadrant suggests a barrier is present at the back contact; no significant shunting is present, and the series resistance is relatively high due to the fact that these are not isolated dot cells and therefore the TCO adds a substantial component to the series resistance. The current densities from the light I-V data suggest J_{SC} 's well above 21-23 mA/cm² (cell areas are 0.1 cm²); the SR data, which is taken at low light intensities, shows a substantial loss in J_{SC} and this is an issue that must be resolved in the future.

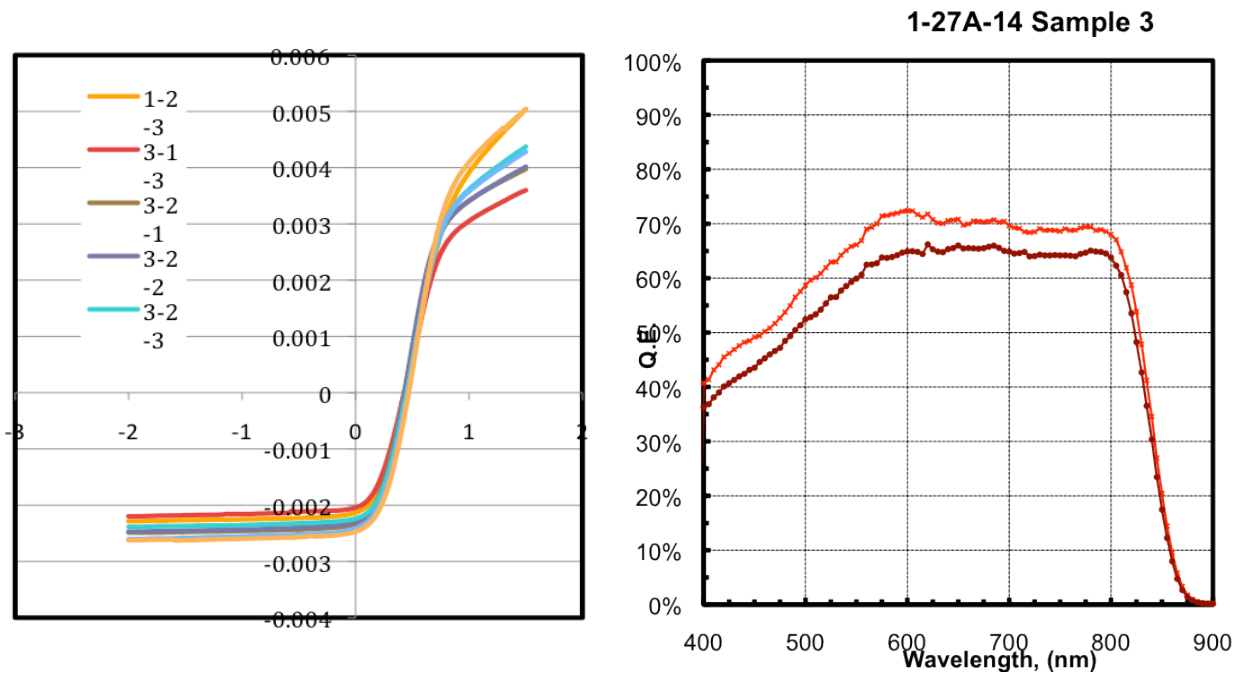


Figure 10. Light I-V and SR data for CdTe cells contacted using polymers (SAMs) as interfacial contact layers; Mo/SAM/CdTe/CdS.

Although, some interesting trends were observed with the use of polymers to modify the work function of Mo, this work remains for all practical purposes very preliminary; many process parameters appear to be critical in studying the effect of polymer interfacial layers; the most critical ones are believed to be the condition of the CdTe surface, the method of application of the polymers, and the polymer properties.

Subsequent experiments included Cu during the cell fabrication process (CuTe_x was deposited by sputtering on the CdTe surface following the Br-methanol etch step); although V_{OC} s increased substantially (low 700's mV) the use of Cu appeared to dominate cell performance "masking" the effect of the polymers. It is believed that additional work on this approach will be valuable and could produce improvements in the contact formation process. Such an effort should be accompanied with surface/interface analysis techniques to characterize the CdTe/polymer/metal interfaces.

5 The Effect of CdTe Impurities on Solar Cell Performance

A considerable effort of this project is dedicated to incorporating impurities in CdTe in order to increase its net doping (hole) concentration and therefore the built-in junction potential and V_{OC} of the solar cells. Several approaches have been considered in order to affect the doping characteristics of CdTe; these included: (a) incorporating phosphorous (P) in the CSS CdTe source material; (b) varying the gas ambient during the CSS-CdTe deposition (relative amounts of O_2 and N_2); (c) diffusion of antimony (Sb) into CdTe following the CdTe deposition by CSS. The following sections summarize the results obtained for each of these cases.

5.1 Phosphorous (P) Incorporation in the CdTe Source Material

This series of experiments was one of the first attempts (at USF) to dope CdTe during the CSS deposition. It must be noted that the CdTe films used for the fabrication of high efficiency cells (at USF) are deposited by CSS in the presence of oxygen (mixture of He and O_2); one of the effects of the use of O_2 during the CSS deposition is more compact grains due to an apparent increase in the nucleation sites; in addition, O_2 is often found to enhance the p-type characteristics of CdTe.

In order to add P to the CdTe source material, powders of CdTe and Cd_2P_3 were mixed and sealed in an evacuated quartz ampoule. The relative amounts of the two powders corresponded to approximately 5% at. of P. The quartz ampoule was subsequently heated to temperatures up to $700^\circ C$. After approx. 48 hrs at this temperature the mixed powder was removed from the ampoule, pulverized and remixed. This powder (to be referred to as P-doped from this point forward) was then used to deposit “CdTe:P” films by CSS (all CSS depositions described in this section were carried out in an inert ambient - 100% He). The first few depositions resulted in unusually non-uniform films; the reason for the observed non-uniformities is believed to be due to inhomogenities in the P-doped powder. In order to improve film uniformity the P-doped powder was used to deposit a thick CdTe film (approx. $300\ \mu m$) onto a glass substrate. This CdTe:P coated glass slide was then used as the source material for the CSS process; prior to using this source material for cell fabrication it was analyzed using EDS. The analysis indicated that 3% at. P was present, which was in relatively good agreement with the amount of P initially introduced in the CdTe powder (5% at.).

A series of CdTe films were deposited onto CdS/SnO₂(bilayer)/glass substrates for solar cell fabrication (CSS conditions: He-ambient; $T_{SUB}=550^\circ C$; $T_{SRC}=630^\circ C$). In order to decouple the effect of the impurities incorporated in the CdTe:P films, some cells were completed without the use of the CdCl₂ heat treatment, and all cells were fabricated with Mo back contacts (i.e. no Cu was used for the fabrication of the back contact).

The characteristics of the completed devices were in general very poor bringing into question the quality of the mixed powders; Figure 11 shows the V_{OC} and FF as a function of the processing conditions. The “best” devices from this group of cells were the ones fabricated using optimum ($390^\circ C$) CdCl₂ conditions clearly indicating that the most critical processing step in this case is the CdCl₂ treatment, and therefore at this time it appears that “P-doping” is not having a beneficial effect on the device characteristics. EDS analysis of one of the CdTe:P films indicated that no P was present. This result does not necessarily suggest that P was completely absent in these films; it is possible that the amount of P incorporated in the film was well below the detection limits of this technique. The tentative conclusion at this time is that P does not

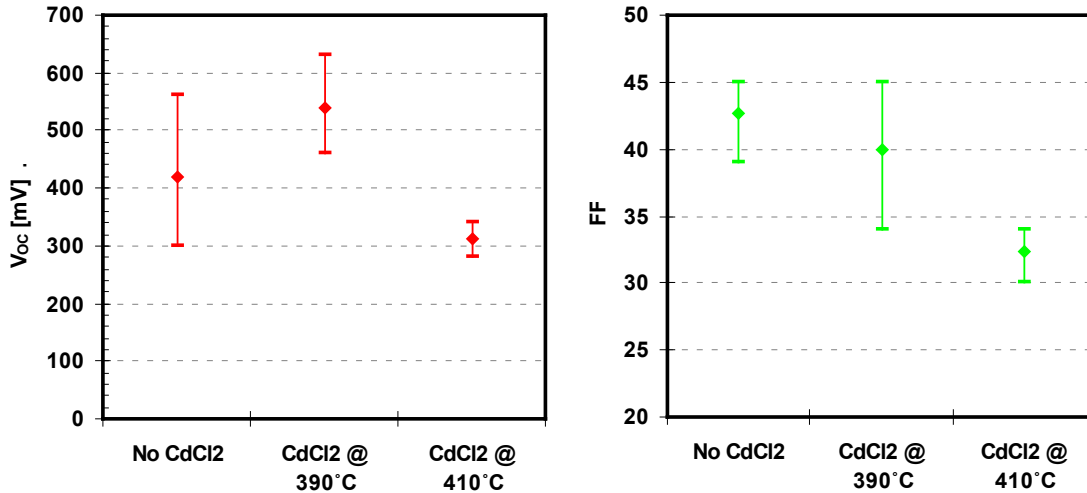


Figure 11. V_{OC} and FF for CdTe cells fabricated from a CdTe:P CSS source

transport at the same rate as CdTe during the CSS deposition process, and the CdTe source may be depleted of P after the first few depositions (possibly by the second or third deposition). Resolving this issue and determining whether P can be incorporated in CSS-CdTe films used for cell fabrication will require further investigation. A series of CdTe:P films has been forwarded to NREL for SIMS analysis.

5.2 The Effect of CSS(CdTe) Ambient

As indicated previously, the CdTe films utilized for the fabrication of high efficiency cells are deposited in an O_2 -containing ambient (He/O_2). During the first year of this project the effect of a N_2 - O_2 CSS ambient on the characteristics of CdTe cells was studied. All devices discussed here were fabricated using baseline fabrication conditions (CBD-CdS; Cu-doped graphite back contact; CdCl₂ heat treatment). The only intentional process variation was the composition of the gas mixture during the CSS-CdTe deposition: The total pressure was fixed at 10 torr, and the relative amounts of N_2 and O_2 were adjusted to result in the following N_2/O_2 ratios: 9/1, 7/3, 5/5, and 1/9. The performance of these devices (V_{OC} and FF) is shown in Fig. 12 (minimum of 3 cells per condition). These results show a clear trend of improving V_{OC} 's and FF with increasing O_2 (decreasing N_2) partial pressure.

Dark J-V characteristics for representative devices are shown in Fig. 13. The $\ln(J)$ -V shown on the left suggest that the device fabricated with CdTe with the lowest O_2 partial pressure has a higher dark current (J_0), which partially accounts for the lower V_{OC} and FF for the cells fabricated with a N_2/O_2 ratio of 9/1. However, the other three

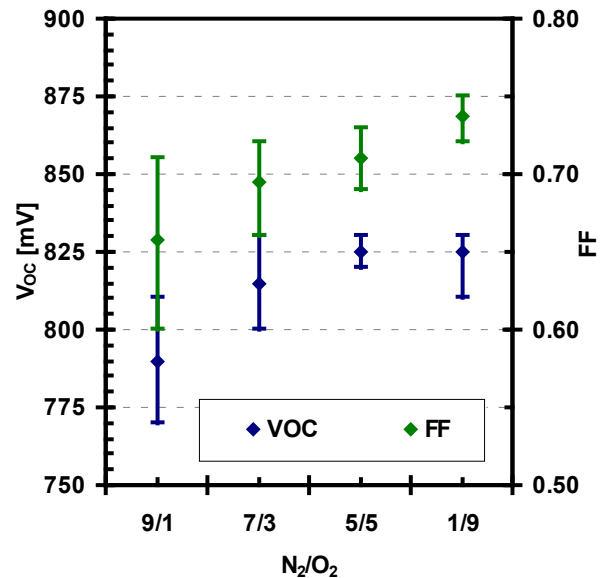


Figure 12. The effect of the CSS-CdTe deposition ambient on the V_{OC} and FF of CdTe solar cells

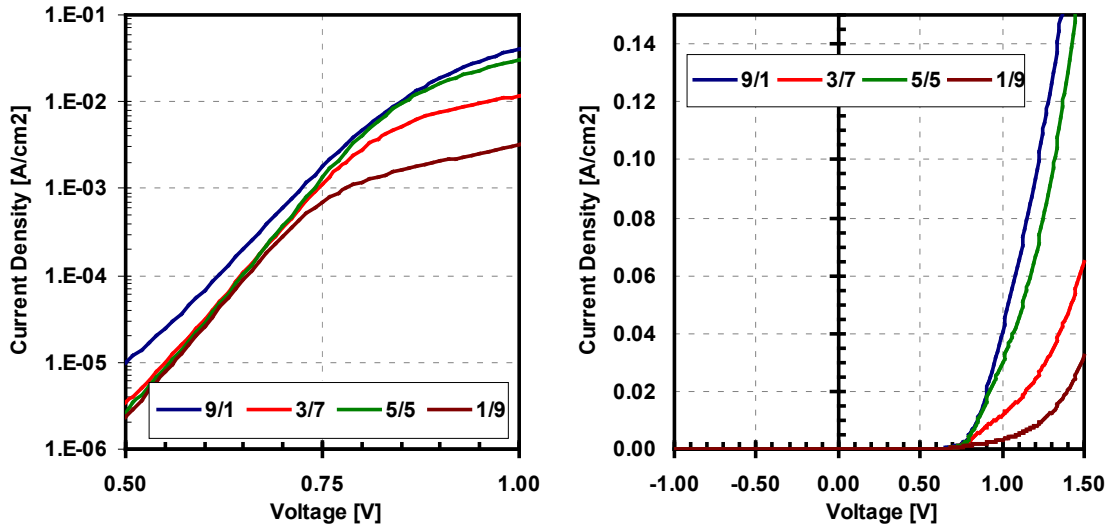


Figure 13. Dark J-V characteristics (left: $\ln(J)$ -V; right: J-V) for representative cells fabricated under various N_2/O_2 mixtures (total pressure 10 torr) during the CSS-CdTe deposition

cells seem to have identical dark currents especially in the range of 0.5-0.75 volts (i.e. near V_{OC}). The dotted line in the same graph marks the J_{SC} magnitude, and assuming superposition it should cross the dark J-V at V_{OC} . Although series resistance effects interfere with the dark J-V characteristics around V_{OC} , all four J-V characteristics seem to be converging around the same value of V_{OC} .

The linear dark J-V shown in Fig. 13 (right) suggest that increasing amounts of O_2 during the CdTe growth lead to a considerable decrease in the forward dark currents beyond V_{OC} (the turn-on voltage of the J-V curve “shifts” to higher voltages). This behavior does not transfer to the light characteristics (i.e. no crossover), and it has been previously attributed to the properties of the CdS films (photoconductivity) and not the properties of CdTe. It is therefore possible that the O_2 used during the deposition of CdTe has an effect on the CdS, since the CdS is exposed to this ambient for approximately 2 minutes prior to the start of the CdTe deposition. The best performers in this group are cells with the largest shift in their dark J-V (i.e. lower forward current at voltages above 1.0 volt). This result seems to point that the observed device performance variations are due to the influence of the CdS and not CdTe, and seems to support a device model where CdS has insulating properties and the device behaves as an MIS structure [14].

The light J-V characteristics for the same

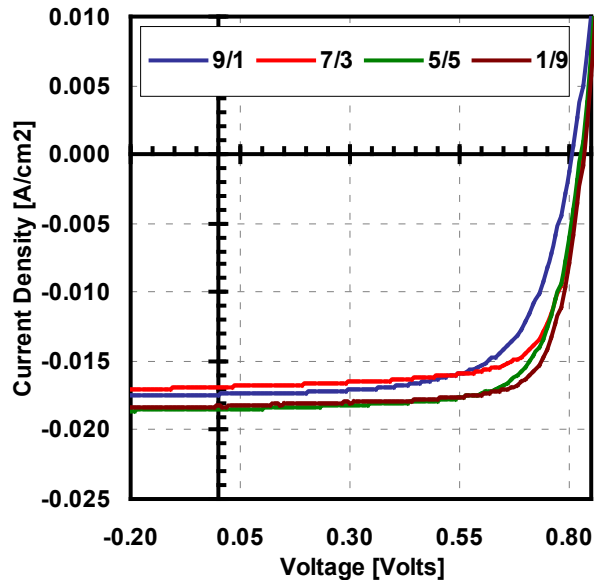


Figure 14. Light J-V characteristics of the CdTe cells of Fig. 11

cells are shown in Fig. 14. These suggest that the lower FF (and V_{OC}), for the device fabricated with a N_2/O_2 ratio of 9/1, is due to softening of the J-V curve around the maximum power point as a result of collection losses, and not due to shunting (shunt resistances calculated at a reverse bias of 1.5-2.0 Volts were very similar for all devices). This suggests that the use of O_2 during the CSS-deposition of CdTe affects the strength of the field in this layer (and therefore collection); at this time it is not clear whether the collection in CdTe is affected by O-incorporation in CdTe, or by the properties of the window layer (CdS), which as indicated above appears to be affected by the use of O_2 during the CdTe deposition.

The same devices (shown in Figs. 13 & 14) were characterized using C-V measurements. The values for the net hole concentration (N_A-N_D) and the depletion width were calculated from the linear portion of the $[1/C^2 \text{ vs. } V]$ graph and the capacitance at 0V bias respectively, and are listed in Table 8. All values for carrier concentration are well within the range typically observed for CdTe devices (i.e. low 10^{14} cm^{-2}). Nevertheless, there appears to be a slight (but consistent) increase in the net hole concentration as the O_2 partial pressure. As previously described (see Fig. 12) the V_{OC} also increased with O_2 partial pressure, by approximately 40-50 mV. To first order it appears that there is a correlation between the net hole concentration and V_{OC} ; this evidence supports the claim that oxygen acts as a p-type dopant in CdTe. However, the increase in doping level is also accompanied by a decrease in the depletion width, which would lead to poorer collection (and therefore lower FF), which is not the case for these cells.

Even though a small increase in carrier concentration is observed, it seems that a “saturation” level is reached for this device property. This is most likely associated with the nature of CdTe, being a II-VI semiconductor, and the fact that self-compensation is often the limiting factor for achieving high doping levels in these materials. It is also evident that the effect of the CSS ambient (oxygen in particular) is rather complex, and based on these results it could be concluded that both the absorber (CdTe) and window layer (CdS) are affected by the presence of O_2 during the CdTe growth. The results clearly suggest that O_2 is beneficial to the CdTe cell, but fully understanding the role of O_2 will require additional studies.

Table 8. Net carrier concentration and depletion width for the cells shown in Figs 13 & 14

| | N_2/O_2 | | | |
|--|-----------------------|-----------------------|-----------------------|----------------------|
| | 9/1 | 7/3 | 5/5 | 1/9 |
| $N_A-N_D [\text{cm}^{-3}]$ | 1.98×10^{14} | 2.77×10^{14} | 3.46×10^{14} | 3.4×10^{14} |
| $W_D @ 0 \text{ Volts } [\mu\text{m}]$ | 3.03 | 1.82 | 1.98 | 2.03 |

5.3 Antimony (Sb) as a Potential Dopant for CdTe

Antimony (Sb) is another group V impurity, which was considered as a potential p-type dopant for CdTe. At this time it should also be noted that Sb_2Te_3 has been used as a back contact material to CdTe solar cells, and therefore it may play a dual role in CdTe i.e. as a dopant and also as a back contact electrode, if the processing conditions lead to the formation of the Sb_2Te_3 compound on the surface of CdTe. Following the results obtained with P, it was decided to attempt to incorporate Sb in CdTe via a post-deposition method, rather than during the CSS deposition process. Following the CSS deposition of CdTe, a thin film of Sb (20-30 nm) was deposited onto CdTe by sputtering. The structures were subsequently heat-treated in inert ambient, in order to cause Sb to diffuse into the CdTe film; annealing temperatures varied from 300 to 525°C, and annealing times from 20 to 160 mins. Some of the early experiments

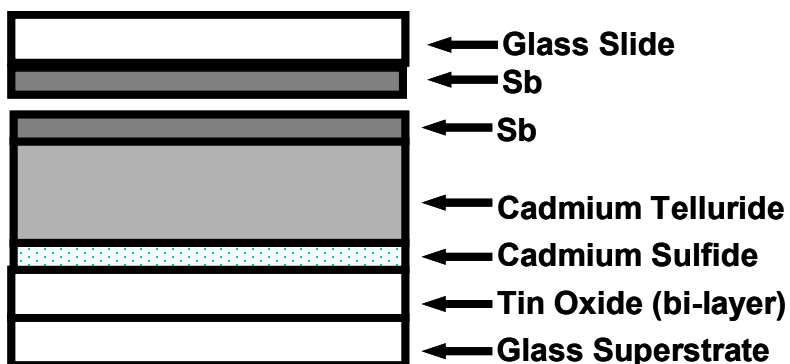


Figure 15. Sample arrangement used for the Sb diffusion experiments. Credit: University of South Florida

suggested that Sb was evaporating from the CdTe surface; in order to limit Sb loss during the heat treatment, an Sb-coated glass slide (with 200-300 nm of Sb) was placed on top of the CdTe for the remainder of the experiments (see Fig. 15); all cells exposed to this process will be referred to as *CdTe:Sb* (or *Sb-doped*). In some instances the CdTe surface was etched in dilute HCl solution in order to remove any Sb remaining on the CdTe surface and eliminate any influence this may have on the formation of the back contact. It is well known that the fabrication process of high efficiency CdTe cells intentionally introduces several impurities in the solar cell, which include copper, chlorine and oxygen. The work described in this section was intended to investigate and understand the role of Sb as a potential p-type dopant. All cells discussed in this section were fabricated with CSS-CdTe films deposited in the presence of O₂ (see O₂ effect in a previous section), and the back contacts were fabricated using molybdenum (Mo) sputter-deposited at room temperature (no Cu was intentionally used during the cell fabrication process).

5.3.1 The Need for the CdCl₂ Heat Treatment (HT)

The improvements in the performance of CdTe solar cells as a result of the CdCl₂ HT are well known. Initial experiments with CdTe:Sb focused on fabricating solar cells with and without the CdCl₂ HT, in order to determine whether this step could be excluded from the cell fabrication process and therefore be able to decouple the effects of Sb from other impurities.

Table 9 lists processing conditions and solar cell performance for CdTe:Sb solar cells. These results are among many that clearly underscore the great importance of the CdCl₂ HT. The improvements in both the V_{OC} and the FF are substantial and in this case translate to an approximate increase in efficiency from a range of 6.5-7.2 to 11.0-11.3%; an increase of 4-5%. At this time it was decided that going forward with the Sb-doping work, the CdCl₂ HT should be included as part of the cell fabrication sequence, simply because its impact on solar cell performance could not be accomplished by other means. However, a substantial number of cells were fabricated without the CdCl₂ HT, in order to try to better understand the role of the various impurities and processes (see table 9 results).

Table 9. Process conditions and solar cell results for CdTe:Sb cells; the effect of the CdCl₂ HT

| Sample ID | “A” | “B” | “C” | “D” |
|--|---|-------------|------------|------------|
| CdTe | In O ₂ ambient; thickness 5-6 μm | | | |
| Sb Thickness on CdTe [nm] | 20 | | | |
| Heat Treatment (Sb Diffusion) T[°C]/time[min] | 400/25 | 450/25 | 430/25 | 430/25 |
| CdCl ₂ HT | None | None | Yes | Yes |
| Contact | Sputtered Mo; | | | |
| V _{OC} [mV] | 710-730 | 740-750 | 800-810 | 810-830 |
| FF [%] | 37-41 | 41-44 | 61 | 61-62 |

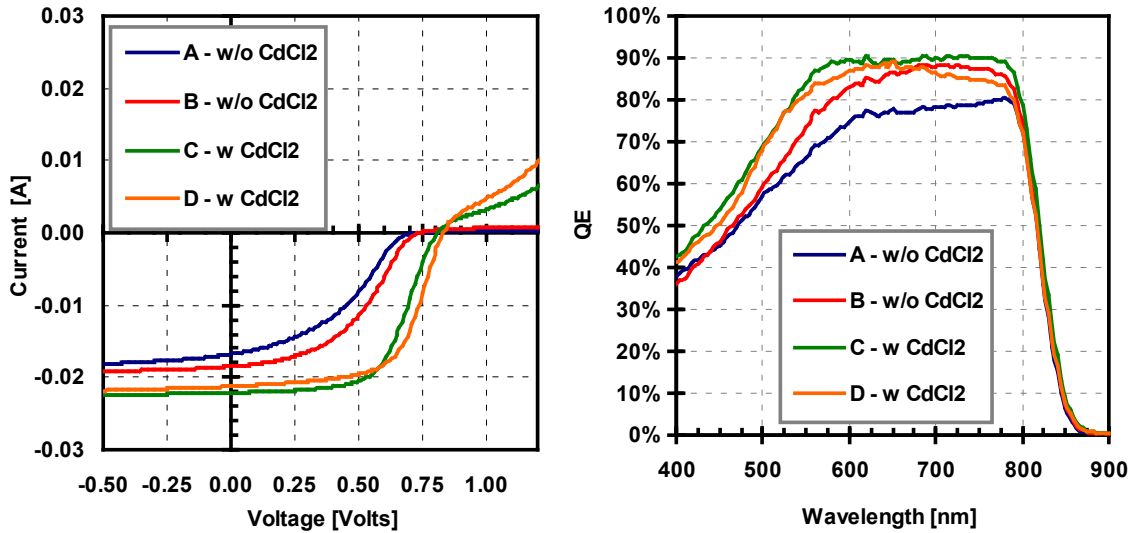


Figure 16. Light J-V (left) and SR data (right) for representative CdTe:Sb cells from table 9

The improvements in performance (due to the CdCl₂ HT) are evident from the light J-V and spectral response (SR) data, for a representative set of cells, shown in Fig. 16. Although, the roll-over (slope around V_{OC}) behavior, indicative of the presence of a back contact barrier, is evident in all cells, it is more severe in the cells not exposed to the CdCl₂ HT. Large enough barriers at the back contact could also result in losses in J_{SC}, which is also the case for the cells fabricated without the CdCl₂ HT.

5.3.2 The Effect of Excess “Surface-Sb”

The next set of cells listed in Table 10 are among those fabricated without the CdCl₂ HT, and in this particular case the objective was to determine whether excess Sb, left on the surface of CdTe after the diffusion-heat treatment, had an effect on the characteristics of the solar cells. In two of the cases listed in Table 10 the solar cells were etched in HCl following the Sb-diffusion process in order to remove excess Sb.

Solar cell performance is poor in all instances (compared to state-of-the-art cells); the reason for the poor performance is as indicated in the results presented above (table 9 & Fig 16) the exclusion of the CdCl₂ heat treatment. Figure 17 shows the light and dark I-V characteristics from representative devices. It is clear, based on the dark and light I-V rollover, that the limiting mechanism in all cells is a large barrier at the back contact. However, cells etched with HCl (to remove excess Sb from the CdTe surface) exhibit consistently lower V_{OC}'s and J_{SC}'s, and their

forward dark currents (beyond the junction turn-on voltage) are suppressed more severely. All these characteristics seem to suggest that the back contact barrier is larger in the case where excess Sb was removed (i.e. cells etched with HCl). It is therefore tentatively concluded that the presence of Sb at the surface of CdTe leads to a reduction in the back contact barrier. Antimony telluride (Sb_2Te_3) has been used by others as an effective back contact material for CdTe [15].

Table 10. Process conditions and performance data for CdTe:Sb cells; the effect of HCl etch

| Sample ID | “400/HCl” | “400/NO HCl” | “450/HCl” | “450/NO HCl” |
|--|---|--------------|-----------|--------------|
| CdTe | In O ₂ ambient; thickness 5-6 μm | | | |
| Sb Thickness on CdTe [nm] | 20 | | | |
| Heat Treatment (Sb Diffusion) T[°C]/time[min] | 400/25 | 400/25 | 450/25 | 450/25 |
| HCl Etch | Yes | No | Yes | No |
| CdCl ₂ HT | None | | | |
| Contact | Sputtered Mo; | | | |
| V _{OC} [mV] | 680-690 | 710-730 | 630-680 | 740-750 |
| FF [%] | 37-38 | 37-41 | 32-37 | 41-44 |

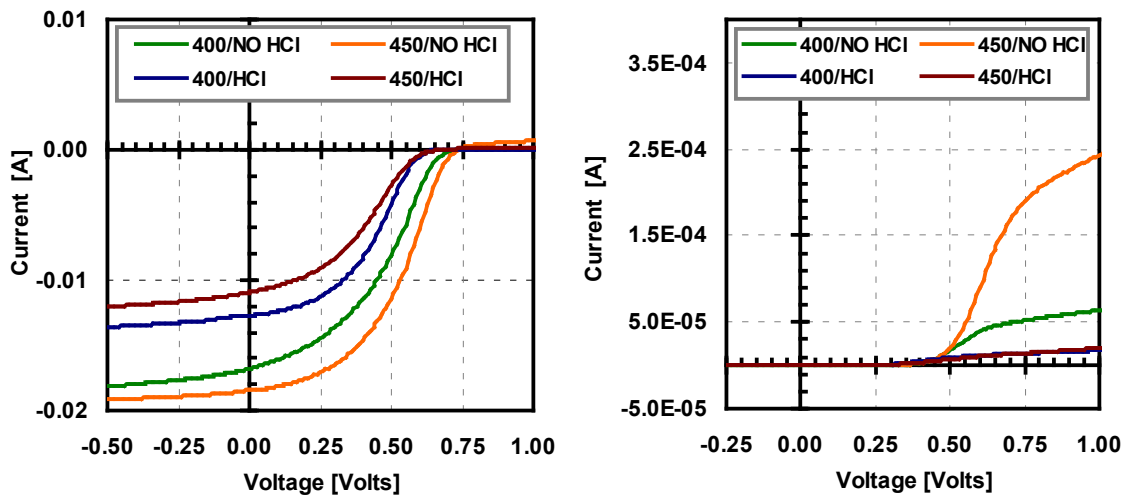


Figure 17. Light (left) and dark (right) I-V for representative CdTe cells from table 10

5.3.3 The Effect of the Sb-diffusion Process Parameters

The optimum conditions for the Sb-diffusion process have not been established; the temperature has been varied from 400-525°C, the time from 20-180 mins, and the thickness of Sb deposited onto the CdTe surface from 20-50 nm; as indicated earlier an Sb-coated glass slide was also placed on the CdTe surface during the Sb-diffusion step.

Table 11 lists the performance data for CdTe:Sb cells for which the annealing time was varied from 40-160 mins. While the annealing time of 40 mins yields the lowest performance cells in this set, annealing times of 80-160 mins result in essentially identical V_{OC}'s and FF's.

Table 11. Process conditions/solar cell results for CdTe:Sb cells; the effect of annealing time

| Sample ID | "40" | "80" | "120" | "160" |
|--|---|---------|---------|---------|
| CdTe | In O ₂ ambient; thickness 5-6 μm | | | |
| Sb Thickness on CdTe [nm] | 30 | | | |
| Heat Treatment (Sb Diffusion) T[°C]/time[min] | 400/40 | 400/80 | 450/120 | 450/160 |
| CdCl ₂ HT | YES | | | |
| Contact | Sputtered Mo; | | | |
| V _{oc} [mV] | 700-730 | 750-770 | 730-770 | 740-770 |
| FF [%] | 58-63 | 60-62 | 61-63 | 61-64 |

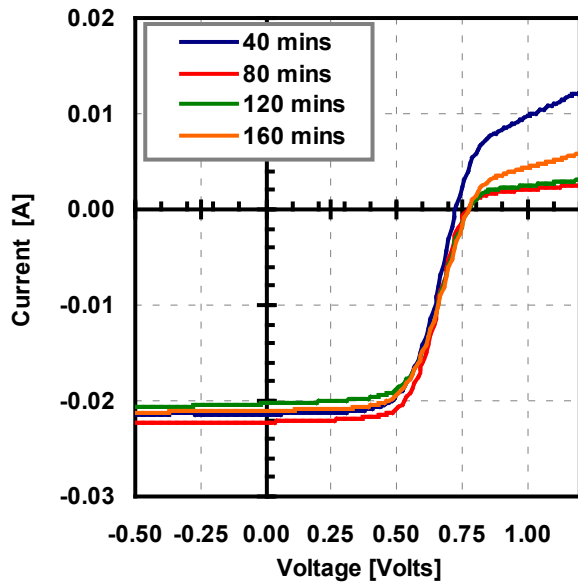


Figure 18. Light J-V for representative cells from table 11

The light J-V for representative cells are shown in Fig. 18. The lowest performer in the group, the cell with the shortest Sb-annealing time, also seems to exhibit the “least” rollover. It is not clear at this time what mechanism causes this behavior, however, it is possible that increased carrier concentration in the CdTe near the back contact for the cells annealed for long times (80-16 mins), results in increased band bending at that interface which will result in a larger barrier for holes (moving from CdTe to the contact). Resolving this issue will require numerical modeling that can consistently capture these differences in these devices. The doping profiles for the same cells are shown in Fig. 19, and they

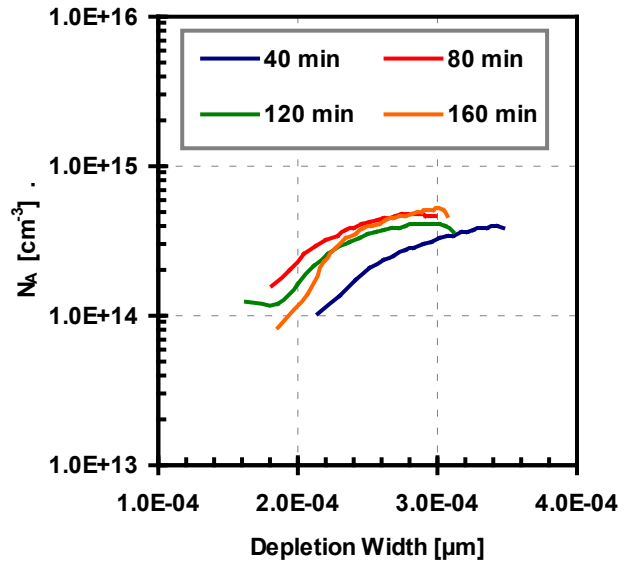


Figure 19. Doping profiles (from C-V measurements) for the cells shown in Fig. 18

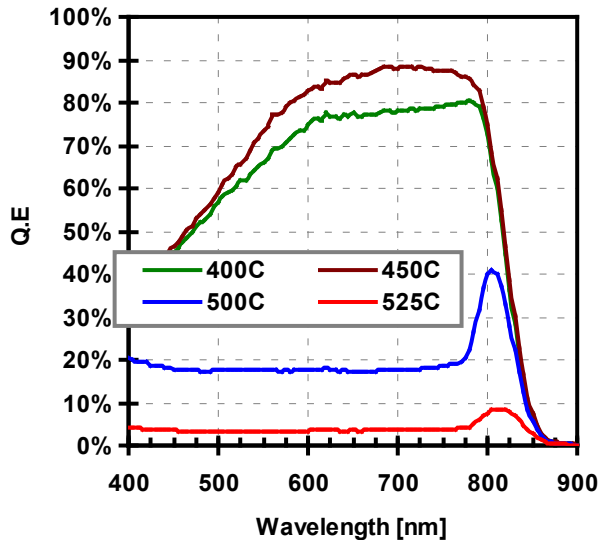


Figure 20. The SR of CdTe:Sb cells fabricated with different Sb-diffusion temperatures

appear to partially support the increased doping claim; the lowest doping levels are observed in the device with the shortest annealing time.

Figure 20 shows the SR of several cells for which the Sb-diffusion time was fixed at 25 mins and the temperature was varied from 400-525°C. These data clearly demonstrate that at high annealing temperatures the collection of carriers decreases dramatically independent of the illumination wavelength. This type of behavior could be explained with increased interfacial recombination. Solar cell performance initially increased (up to 450°C); however, above 450°C the performance became “noisy” (i.e. increased scattering in performance data) and clearly decreased above 500°C. Based on these results the annealing temperatures were limited in the 400-450°C range for most experiments.

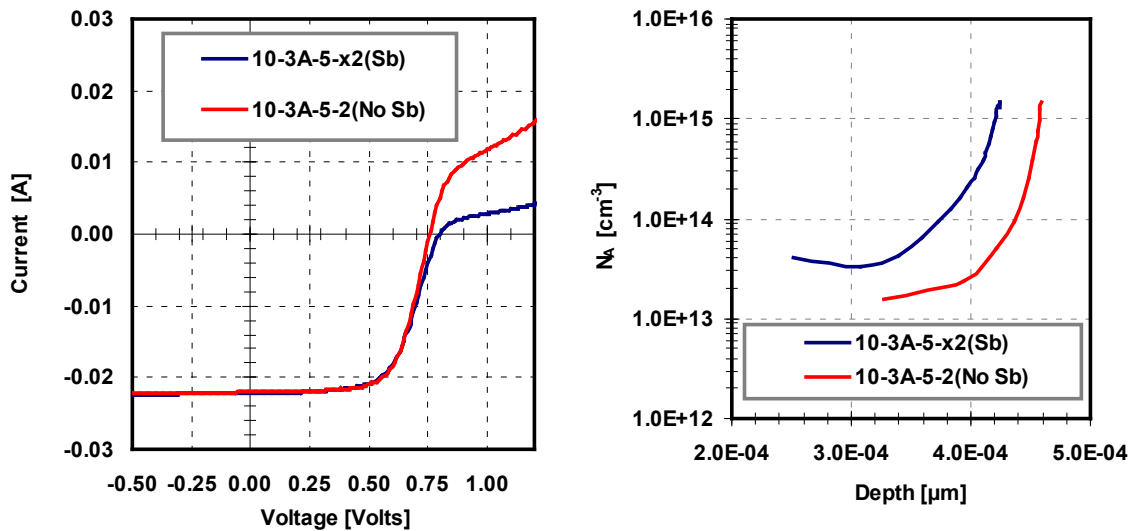


Figure 21. Light J-V (left) and doping profile (right) of CdTe cells fabricated with and w/o Sb-diffusion

Based on the to-date results with Sb-diffusion, it appears that effective doping of CdTe (i.e. $>10^{15} \text{ cm}^{-3}$) is yet to be accomplished with this approach. Even though in several experiments there is consistent increase in the hole concentration, the doping levels measured were always within the general range typical of CdTe devices (fabricated w/o Sb) i.e. 10^{14} cm^{-3} . In general Sb may present a unique opportunity for CdTe devices, since it appears to potentially benefit the back contact region of the device (i.e. CdTe surface) as well as the bulk doping of CdTe. From a stability point of view, it may lead to the elimination of Cu from device processing, an element that is often suspected to be responsible for device degradation. Figure 21 shows light J-V characteristics and the CdTe doping profile for cells fabricated on the same substrate, in order to eliminate experimental variations/errors. The only processing difference between the two is that one of the devices was subjected to the Sb-diffusion process. It is clear that both the V_{OC} and the doping levels in the CdTe:Sb device are higher (the V_{OC} by 50 mV), suggesting that increasing the doping in CdTe further could potentially yield even higher V_{OC} 's as expected.

6 Indium (In) Doped CdS

Another activity undertaken under this project dealt with using intentionally doped CdS films for the fabrication of CdTe/CdS solar cells, in order to determine whether increasing the n-type conductivity of CdS could be beneficial to solar cell performance. In theory, one would expect that an increase in the net doping in either heterojunction partner to lead to an increase in the built-in potential and therefore V_{OC} . However, it has been previously found that a compensating impurity in this material (CdS), such as Cu, leads to improved performance [9]; others have also proposed a device operation model to explain how device performance can benefit from a compensated or “insulating” CdS[14].

For this project In was introduced in CdS films in two ways as shown in Fig 22: (a) by depositing In onto the SnO₂/glass substrate before the CdS deposition by CSS; by depositing In onto (b) CSS-CdS or (c) CBD-CdS; and (d) by depositing CSS-CdS from an In-doped CdS source (purchased with In). In the first 3 cases, the substrates were annealed prior to the deposition of CdTe.

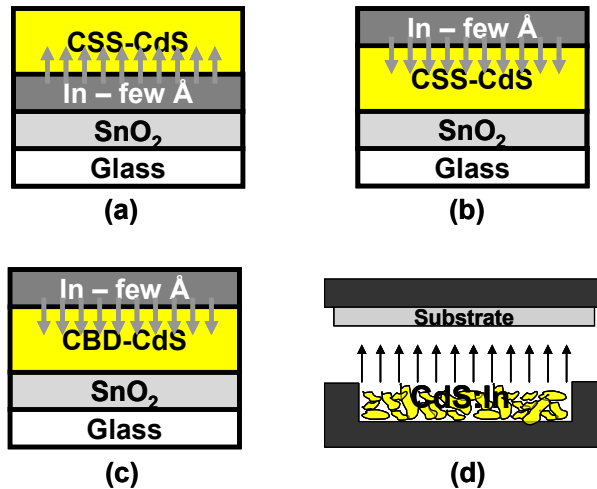


Figure 22. Methods used to incorporate indium in CdS

6.1 CBD-CdS Control Samples

The first few experiments to dope CdS with Indium, utilized CBD-deposited CdS films, in order to establish a baseline for device performance. Indium was sputtered at room temperature onto CBD-CdS at two thicknesses 5 and 10 Å. The films were subsequently processed into solar cells using “baseline” processes.

Table 12. CdTe Solar Cells fabricated with CBD-CdS films as-deposited and doped with Indium

| CBD-CdS:In Cells | | | | | Baseline Cells | | |
|------------------|----------------------|--------|----------------------|--------|----------------|----------------------|--------|
| Cell ID | V _{oc} [mV] | FF [%] | Indium Thickness [Å] | Anneal | Cell ID | V _{oc} [mV] | FF [%] |
| 5-17a-6-1 | 770 | 45 | 10 | Y | 5-17a-6-x1 | 820 | 71 |
| # 2 | 750 | 46 | | | # x2 | 810 | 72 |
| # 3 | 760 | 47 | | | # x3 | 810 | 72. |
| 5-17a-7-1 | 530 | 48 | 10 | N | 5-17a-7-x1 | 820 | 68 |
| # 2 | 530 | 45 | | | # x2 | 810 | 69 |
| # 3 | 530 | 42 | | | # x3 | 810 | 72 |
| 6-6a-4-1 | 780 | 67 | 5 | Y | 6-6a-4-x1 | 830 | 71 |
| # 2 | 760 | 67 | | | # x2 | 830 | 71 |
| # 3 | 760 | 67 | | | # x3 | 830 | 72 |
| 6-6a-5-1 | 780 | 69 | 5 | N | 6-6a-5-x1 | 820 | 73 |
| # 2 | 760 | 69 | | | # x2 | 820 | 73 |
| # 3 | 750 | 67 | | | # x3 | 820 | 73 |

Annealing, following the deposition of In onto CdS (for In in-diffusion), appears to be beneficial, although at the small In thickness (of 5 Å), there is no apparent benefit to device performance. This may suggest that the excess In in the devices (with 10 Å of In) which were not annealed, may have resulted in increased interface recombination, or may have diffused into the CdTe side of the junction resulting in a buried homojunction; SR measurements seem to support the former (i.e. increased interfacial recombination), as shown in Fig. 21; the sample with 10 Å of In (not annealed) exhibits a wavelength independent reduction in its SR.

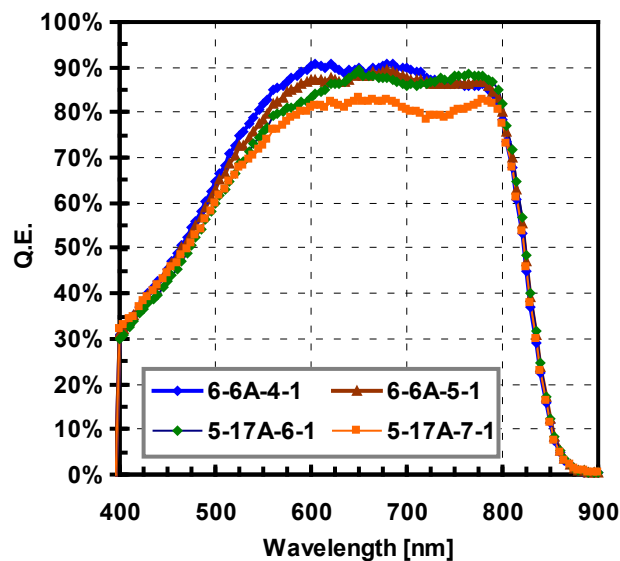


Figure 23. SR data for CdTe cells fabricated with CBD-CdS:In window layers (see table 12)

Even though, the “control” experiment suggested that the incorporation of indium in CdS resulted in decreased performance, similar experiments were carried out with CSS-CdS films. It should be noted that under a previous project, the effect of Cu incorporation in CdS was investigated; in that case the best approach to controllably introduce small amounts of Cu in CdS was by dipping the samples in a CuCl solution; Cu sputtering (similar to the approach taken here to introduce In in CdS) appeared to introduced excessive amounts of Cu and was ineffective.

Introducing In in CdS using a similar approach (i.e. solution of In salts) has not produced noteworthy results.

6.2 In Doping of CSS-CdS

The deposition of CdS by the close-spaced sublimation has been studied under past projects. A key finding was the beneficial effect of deposition CdS in the presence of oxygen. For the CdS:In experiments described in this report CSS-CdS films were prepared in either inert or O₂-containing ambient. Indium was deposited by sputtering at room temperature to thicknesses of 1, 2.5, 4, and 10 Å; even at these small thicknesses the amount of indium in CdS is on the order of 0.2-2% which is relatively high for doping purposes.

Figures 24 and 25 show V_{OC} and FF data (2-3 cells per condition) for cells for which the CSS-CdS was deposited in O₂-ambient (Fig. 24) and in inert ambient (Fig. 25). It is rather difficult to draw any conclusions on the effect of the relative amount of In based on these results, although it appears that the best cell (V_{OC}/FF 810mV/72%) was fabricated with CSS-CdS(O) and the least amount of In (i.e. 1 Å), suggesting that In-incorporation in CdS is actually detrimental to device performance (at least at this high levels). Clearly the most important process parameter is the CSS-CdS ambient; the results confirm past findings where it was demonstrated that cells fabricated with CSS-CdS(O) are better performers than cells fabricated with CSS-CdS deposited in inert ambient.

Spectral response measurements for the cells in Figs 24 and 25 are shown in Fig. 26. In this case there is clear evidence of photocurrent loss with increasing In. Initially the loss appears to be wavelength independent, but eventually exhibits some wavelength dependency suggesting increased deep losses; the photo-current losses observed are not optical, and variations in the thickness of CdS (varying blue QE) are not intentional; CSS CdS films exhibit both spatial thickness variations within the same substrate (on the order of 10-20%), as well as some run to run variations.

All solar cell results obtained to-date suggest that CdS doped with In does not yield improvements in device performance due to potential In diffusion into CdTe or inefficient doping of CdS; the former is very likely due to the high processing temperatures used for solar cell fabrication, and it would lead to additional compensation in CdTe. These issues should be addressed by analyzing CdS:In films and junctions with methods that will provide information on the location and amount of In incorporated in the films and devices; both films and junctions have been forwarded to NREL for SIMS analysis.

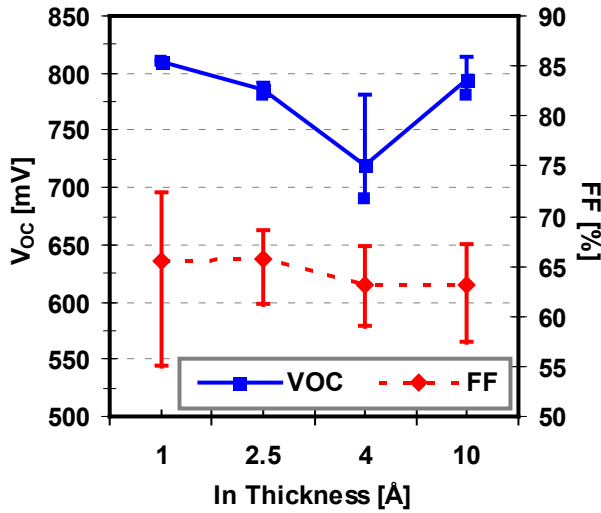


Figure 24. V_{OC} and FF for cells with CSS-CdS deposited in the presence of oxygen

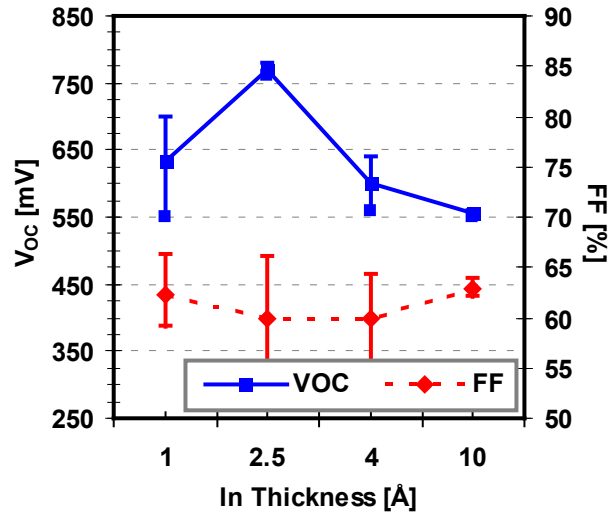


Figure 25. V_{OC} and FF for cells with CSS-CdS deposited in inert ambient

7 Measuring Collection in CdTe Cells

During this project a series of solar cells were evaluated using monochromatic light J-V measurements. We used these data to perform simple analysis on the J-V characteristics of the device and measure the impact of inefficient collection on diode and solar cell parameters.

Figure 27 shows two sets of monochromatic light J-V data for typical CdTe solar cells (FF=69-72%; V_{OC} >810 mV). The interference filters used for these measurements had a bandwidth of 20 nm; and the light intensity was adjusted to correspond to AM1.5 within that bandwidth (i.e. if the entire spectrum was covered the sum of the monochromatic J_{SC} s would add up to the AM1.5 J_{SC}). Figure 28 is a plot of the FF for these two cells (Fig. 27) as a function of wavelength; the dotted lines mark the “white” FF of the devices (i.e. for 100 mW/cm² AM1.5 intensity).

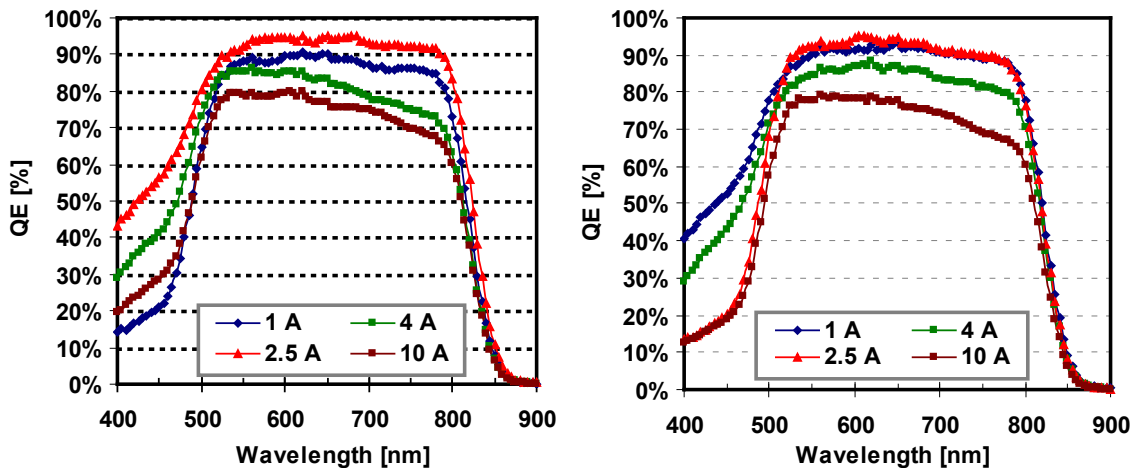


Figure 26. SR data for the cells of Figs 24 (left) and 25 (right)

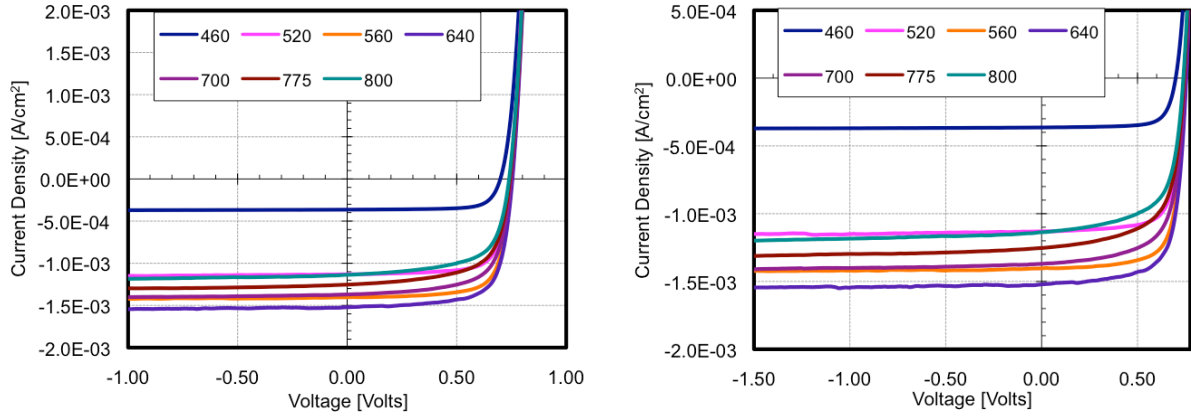


Figure 27. Monochromatic light J-V data for two “typical” CdTe solar cells.

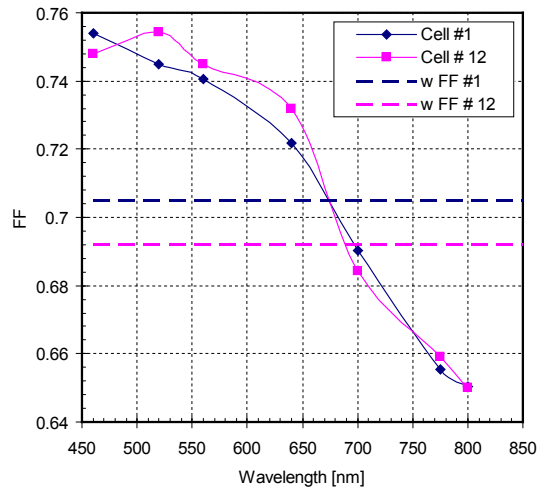


Figure 28. FF as a function of wavelength of the monochromatic light (data from Fig 27).

It is clear that the FF decreases as the wavelength is increased, suggesting that carriers generated by deeply absorbed photons are not effectively collected. The AM1.5 FF lies between the two extreme values measured with monochromatic light; 65 and 75% for 800 and 460 nm respectively. These results clearly suggest that the FF (and V_{OC}) are hampered by inefficient collection. It is therefore suggested that improved transport in CdTe would also benefit the V_{OC} of the CdTe cell.

7.1 The Effect of Collection on Solar Cell Performance

Assuming that collection at 520 nm is 100%, the data in Fig. 27 were normalized, and a “collection” function vs. voltage was obtained by dividing all other J-V data by the 460 nm set. These “collection” functions are shown in Fig. 29; collection for 520 nm is 100% (this was the original assumption), and collection for all other wavelengths decreases with the wavelength.

Two of the collection functions (for 640 and 700 nm) were also fitted with polynomial expressions (as shown in Fig. 29).

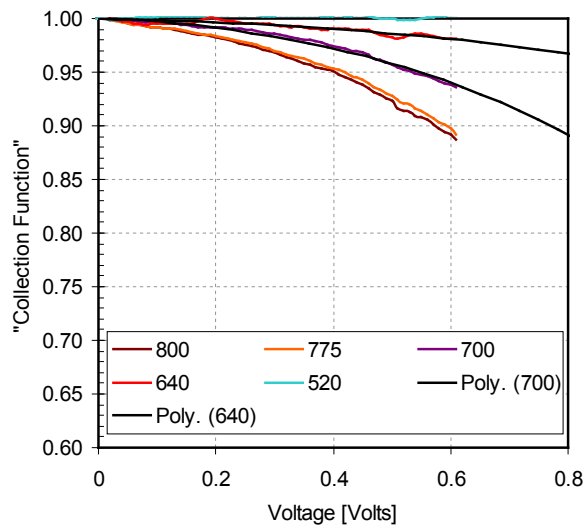


Figure 29. Collection functions for various wavelengths; the data for 640 and 700 nm are fitted with polynomials.

The two fitted collection functions (H(640) and H(700)) are shown in Fig. 30 along with light J-V data for three cells; the dark blue data points represent an ideal device, and the green and red data represent non-ideal cells with collection losses corresponding to functions H(640) and H(700) respectively. The FF for the ideal device is 83% and decreases to 81 and 75% for collection functions H(640) and H(700) respectively. This simple analysis clearly demonstrated the potential advances in efficiency for the CdTe cell if collection (i.e. transport) in CdTe could be further improved.

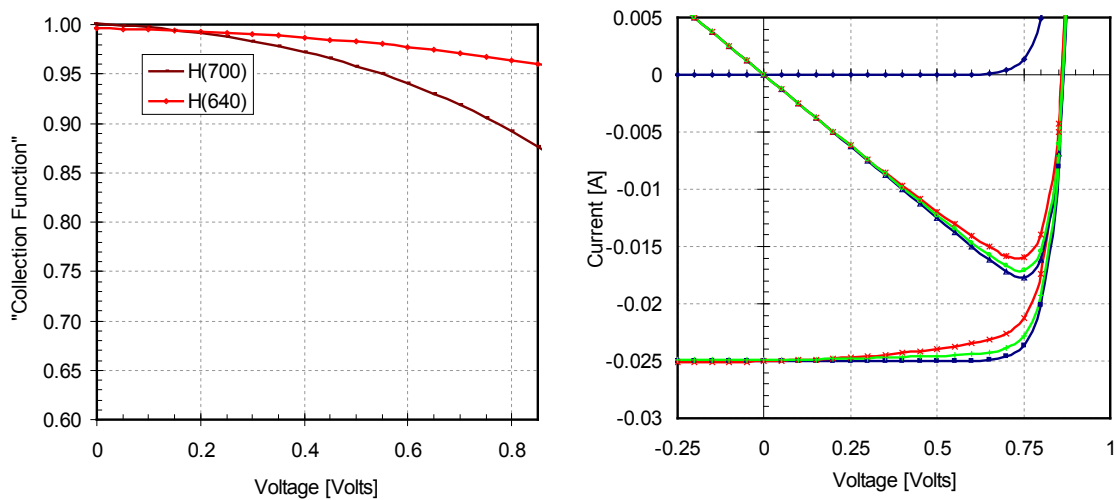


Figure 30. Collection functions for 640 and 700 nm and their effect on the light I-V of an otherwise “ideal” solar cell.

Table 13. Effect of collection on the FF

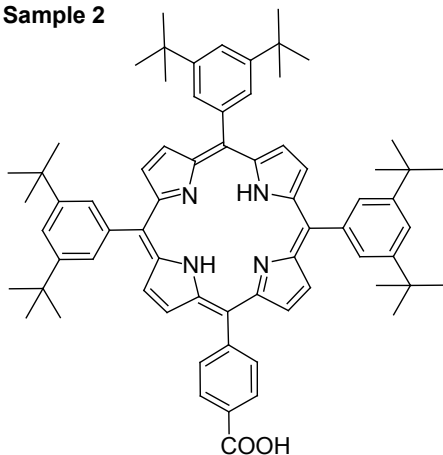
| Ideal Solar Cell | With H(640) | With H(700) |
|-------------------------|--------------------|--------------------|
| 83.3% | 80.8% | 74.9% |

Appendix – Polymers Used as IFLs in CdTe Cells

Sample 1(reference)

Ethanol: CH₃CH₂OH

Sample 2

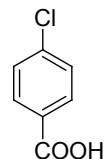


Chemical Formula: C₆₉H₇₈N₄O₂
 Exact Mass: 994.6125
 Molecular Weight: 995.3832

**IV-283-1B 5mg/mL (0.005mol/L),
 Tetrahydrofuran as solvent**

Tetrahydrofuran:

Sample 3

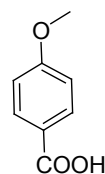


Electron positive

Chemical Formula: C₇H₅ClO₂
 Exact Mass: 155.9978
 Molecular Weight: 156.5664

IV-212A 0.2mol/L in ethanol

Sample 4

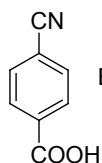


Electronegative

Chemical Formula: C₈H₈O₃
 Exact Mass: 152.0473
 Molecular Weight: 152.1473

p-Anisic acid 0.05mol/L in ethanol

Other sample:

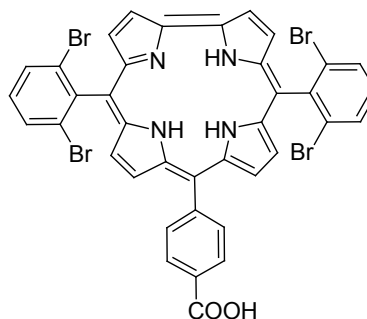


Electron positive

Chemical Formula: C₈H₅NO₂
 Exact Mass: 147.032
 Molecular Weight: 147.1308

Samples: IV-284-1A 0.2mol/ml 5ml(Ethanol)
 IV-284-1B 0.1mol/ml 5ml(Ethanol)
 IV-284-1C 0.05mol/ml 5ml(Ethanol)

new sample:



Chemical Formula: C₃₈H₂₂Br₄N₄O₂
 Exact Mass: 881.8476
 Molecular Weight: 886.2229

**V-100 4.4mg/mL (0.005mol/L),
 Tetrahydrofuran as solvent**

References

1. X. Wu, J. C. Keane, R. G. Dhere, C. DeHart, D. S. Albin, A. Duda, T. A. Gessert, S. Asher, D. H. Levi, P. Sheldon, "16.5%-Efficient CdS/CdTe Polycrystalline Thin-Film Solar Cell", Proc of 17th European PVSEC, (2001) pp. 531-534
2. X. Wu, S. Asher, D. H. Levi, D. E. King, Y. Yan, T. A. Gessert, and P. Sheldon, "Interdiffusion of CdS and Zn₂SnO₄ layers and its application in CdS/CdTe polycrystalline thin-film solar cells", Journal of Applied Physics, 89, 8, (2001), pp. 4564-4569
3. C. S. Ferekides, R. Mamazza, U. Balasubramanian, and D. L. Morel, "Transparent Conductors and Buffer Layers for CdTe Solar Cells", *Thin Solid Films*, 480-481, (2005) pp. 224-229
4. S. Gayam, S. Bapanapalli, H. Zhao, L. Nemani, D. L. Morel and C. S. Ferekides, "The Structural and Electrical Properties of Zn-Sn-O Buffer Layers and their Effect on CdTe Solar Cell Performance", *in print Journal of Thin Solid Films (2007)*
5. Gloeckler, M. Fahrenbruch, A.L. Sites, J.R., "Numerical modeling of CIGS and CdTe solar cells: setting the baseline", proc. 3rd WCPEC, (2003), pp. 491-494
6. K. Durose, S. Asher, W. Jaegermann, D. Levi, B. McCandless, W. Metzger, H. Moutihno, P. Paulson, C. Perkins, J. Sites, G. Teeter, and M. Terheggen, "Physical Characterization of thin film solar cells", Progress in Photovoltaics, 12, (2004), pp. 177-217
7. K. Barri, M. Jayabal, H. Zhao, D. L. Morel, S. Asher, J. W. Pankow, M. R. Young, and C. S. Ferekides, "Introduction of Cu in CdS and Its Effect on CdTe Solar Cells", Proc. of the 31st IEEE PVSC, (2005), pp. 287-290
8. B. Tetali, V. Viswanathan, D. L. Morel and C. S. Ferekides, "Effects of Thermal Stressing on CdTe/CdS Solar Cells", presented at the 29th IEEE PVSC, New Orleans, LA, May 19-24, 2002.
9. S. Erra, C. Shivakumar, H. Zhao, K. Barri, D. L. Morel and C. S. Ferekides, "An Effective Method of Cu Incorporation in CdTe Solar Cells for Improved Stability", *in print Journal of Thin Solid Films (2007)*
10. D. Kraft, U. Weiler, Y. Tomm, A. Thissen, A. Klein and W. Jaegermann: "Alternative back contacts for CdTe solar cells: a photoemission study of the VSe₂/CdTe and TiSe₂/CdTe interface formation", *Thin Solid Films* 431 pp. 382-386 (2003)
11. R. H. Friend, S. S. P. Parkin and D. Jerome: "The Transport-Properties of Vanadium-Doped Tise₂ under Pressure", *Journal of Physics C-Solid State Physics* 15 (25), pp.L871-L874 (1982).
12. Frey, G. L., K. J. Reynolds, and R. H. Friend, *Adv. Mater.* 14, 4, (2002) p 265
13. K. J. Reynolds, G. L. Frey, and R. H. Friend, *Applied Physics Letters*, 82, 7, (2003), p 1123
14. V. G. Karpov, Diana Shvydka, and Yann Roussillon, "Physics of CdTe Photovoltaics: from Front to Back", MRS Spring Meeting 2005, March 28 – April 1, San Francisco, CA
15. D. L. Bätzner, A. Romeo, H. Zogg, R. Wendt, A.N. Tiwari "Development of efficient and stable back contacts on CdTe/CdS solar cells" *Thin Solid Films*, 387, 1-2, (2001) pp. 151-154
16. Dert de Boer, A. Hadipour, M. M. Mandoc, T. van Woundenbergh, and P. W. M. Blom, "Tuning of Metal Work Functions with Self-Assembled Monolayers", *Adv. Mater.*, 17, 5, (2005), 621